POLITECNICO DI TORINO

Corso di Laurea Magistrale
in Ingegneria Meccanica

Modelling and experimental investigation of a two-phase closed thermosyphon heat exchanger coupled to an Organic Rankine Cycle (ORC) system for waste heat recovery

Relatore

Prof. Marco Carlo Masoero

Candidato

Luca Gnaccarini

Aprile 2018

Abstract

Modelling and experimental investigation of a two-phase closed thermosyphon heat exchanger coupled to an Organic Rankine Cycle (ORC) system for waste heat recovery

This work investigates the possibility of coupling an Organic Rankine Cycle (ORC) system for waste heat recovery with a two-phase closed thermosyphon heat exchanger (or gravity-assisted heat pipes or wickless heat pipes). This last component exploits a technology that, from a theoretical point of view, appears to be particularly suitable for conveying heat from exhaust gas of industrial processes to an organic compound used as working fluid in a Rankine cycle, thus allowing the conversion of waste heat into electricity and the consequent reduction of CO_2 emissions.

In the first chapter the objectives of the work will be illustrated and the advantages related to this technology will be presented both from an environmental point of view and from the efficiency of industrial processes. A theoretical study of a two-phase closed thermosyphon is then carried out in the second chapter, by describing the operating principle and providing all the useful information for calculating the performances. Finally, in the third part an experimental investigation on a prototype, which presents similarities with a two-phase closed thermosyphon, will be conducted in order to collect useful data to characterize the behaviour of such technology and identify the most critical aspects.

List of Contents

List of Figures

List of Tables

1 Introduction

1.1 General framework

The European Union (EU) has set a 20% energy saving target for 2020 (compared to 1990) and a dedicated directive [1] on Energy Efficiency to define a set of constraining measures to help European countries reach it. Furthermore, on November 2016 the European Commission proposed an update to the Energy Efficiency Directive, including a new 30% energy efficiency target for 2030. Following these directives, capturing and converting industrial heat losses into electricity is currently arousing much attention. This permits to reduce not only the thermal pollution, due to the direct release of this thermal waste into the environment, but also to improve energy efficiency of the industrial processes [2]. Energy efficiency is certainly a valuable parameter for ensuring sustainable and safe energy supply, reducing greenhouse gases (GHG) emissions and increasing the economic growth and the competitiveness of industry [3].

In many industries, e.g. iron & steel, glass and cement industry, a large amount of energy, generated during a combustion process or several other thermal processes, is often lost as waste heat and directly released into the atmosphere. These waste heat sources not only contain a considerable value of thermal energy but also a large quantity of pollutants: e.g. CO2, NOx, SOx, etc., which are responsible for environmental harmful impacts, e.g. global warming, acid rain etc. [4].

1.2 Objective

The aim of this project is to evaluate the performance of a traditional two-phase closed thermosyphon heat exchanger (or gravity-assisted heat pipes or wickless heat pipes) used for conveying heat from the exhaust stream of a rolling mill Reheating Furnace (RHF) to an ORC (Organic Rankine Cycle) working fluid.

In practice, an intermediate heat carrier loop (e.g. pressurized water, saturated steam or thermal oil loop) is often used to transfer heat from exhaust stream to ORC systems [5]. However, using a heat carrier loop increases the complexity as well as the investment and the operating cost of the global system. A direct exchange between hot exhaust stream and ORC working fluid may be used to improve the cycle efficiency and to reduce costs by eliminating the pumps, heat exchangers and the additional heat carrier loop. However, the installation of the ORC evaporator directly in the hot gas path raises concerns about the decomposition of the organic working fluid at high temperature as well as the safety issue due to the flammability and/or toxicity of organic compound [5], [6]. Using a two-phase closed thermosyphons connected to an ORC system allows to improve the cycle efficiency and to eliminate the costs of the intermediate heat transfer loop, preserving at the same time the organic working fluid from the direct interaction with the hot gases.

So far, there are not many researches on using two-phase closed thermosyphons for transferring heat from exhaust stream to ORC system. The combination between ORC and wickless heat pipes or two-phase closed thermosyphons is only reported in some patents [6], [7]. In the first patent [6], a special type of heat pipe, i.e. inorganic coated heat pipe or also called Qu-type heat pipe, is used for transferring heat from heat source, e.g. exhaust gases, to an ORC working fluid. As described in this patent, Qu-type heat pipes are a type of solid-state heat pipe which operates somewhat similarly to a two-phase closed thermosyphon but do not use a fluid-vapour material to transfer heat from one end to another end of the pipe. In a Qu-type heat pipe, the internal heat transfer material comprises three layers of various combinations of metals such as: Sodium, Beryllium, Manganese, Aluminium, Calcium, etc. The three layers can be applied to a conduit to form devices able to transfer heat. In the second patent [7], the two-phase closed thermosyphons were used to recover the heat from fumes or exhaust gases by using an ORC system or a heat pump or a thermoelectric module. As claimed in the patent, the evaporator section of one or more two-phase closed thermosyphons are submersed in one fluidized bed of sand. The sand, with an average size of about 400 μm, improves the heat transfer between fumes and thermosyphons walls. Both technologies present the advantages for transferring the heat from hot fumes or exhaust gases to ORC working fluid. However, they also present some disadvantages such as high manufacturing cost for Qu-type heat pipes, high cost and an elevated pressure drop for the combination between a fluidized bed of sand and two-phase closed thermosyphons.

It is for the reasons described above that it has been decided to investigate a solution that could simultaneously reduce the costs and complexity of the plant while achieving an efficient heat exchange.

1.3 Steel industry

In steel industry, which is energy-intensive since its production processes are often performed at high temperature, the most efficient way to use the recovered energy is for direct heating purposes, e.g. hot water production. Hot water can be either supplied to external consumer, such as district heating networks or used internally for heating purposes.

However, the best operating practice for flexible heat recovery is probably steam generation, because [4]:

- Steam can be used for many purposes (i.e. process steam, heating, compressor operation and power generation)
- It can operate over a wide temperature range
- Steam is relatively easy to transport
- Water is an inexpensive and is a non-toxic base

When there are no other economically effective uses for the waste heat, its conversion to a more transportable form of energy, such as electricity, must be evaluated.

In steelmaking plants, the largest waste heat potential is produced in the Electric Arc Furnace (EAF) and in the Reheating Furnace (RHF) [3]. Since the EAF uses an electric arc for heating the material, it is not suitable for the application analysed in this study and only the Reheating Furnace has been taken into consideration.

Reheating furnaces are used to heat the steel stock (billets, blooms or slabs) in hot rolling mills to temperature of around 1200°C which is suitable for plastic deformation of steel. During the heating process, which is a continuous process (Figure 1), the steel stock is loaded at the furnace entrance, heated in the furnace and finally discharged.

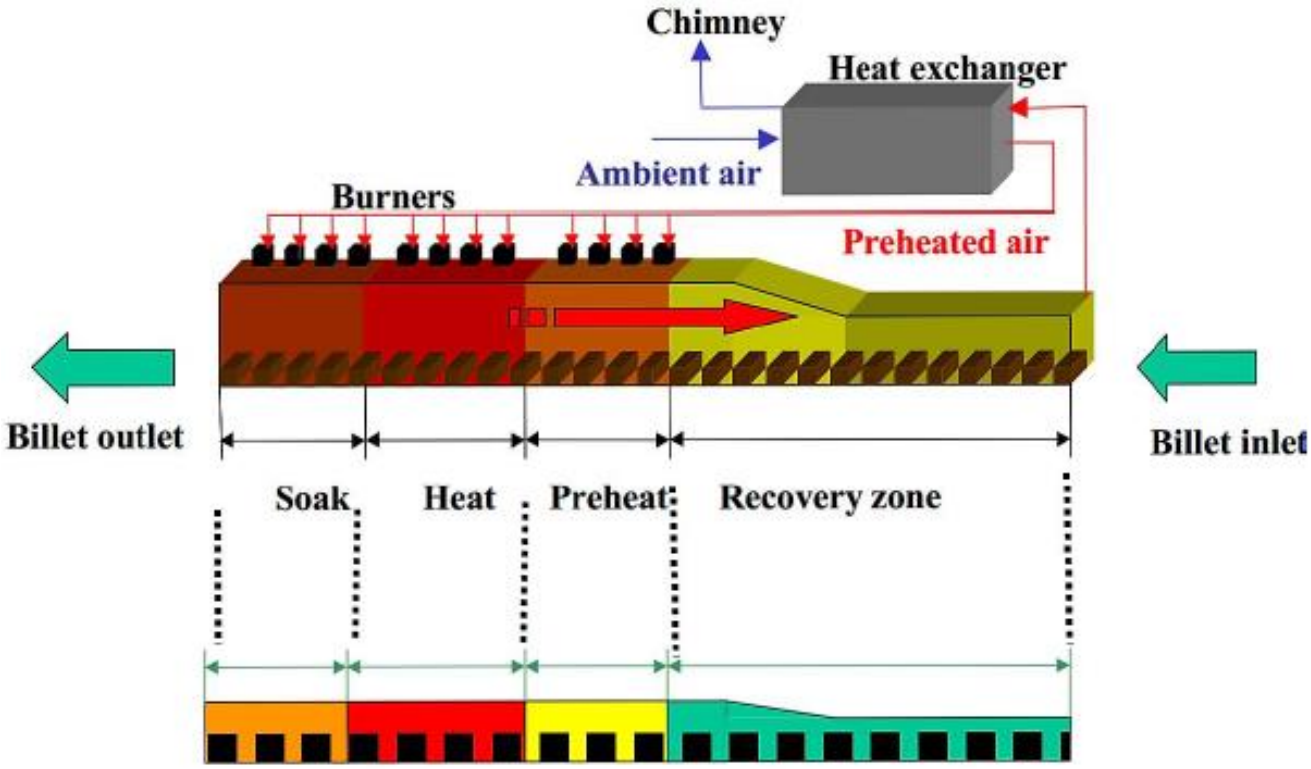

Figure 1. Reheating furnace [1]

In addition to many other feature designs of the furnace such as type of burners, furnace dimensions, number of furnace zones, type of wall and roof insulation, a recovery heat exchanger is usually installed to preheat combustion air by hot flue gases coming out from furnace exit. This shrewdness allows to improve the energy efficiency of the process. The studied reheating furnace has already this kind of recovery heat exchanger (air-preheater) for preheating the combustion air taken from the environment. The additional waste heat recovery system (ORC radiator system) is placed upstream of the air preheater to exploit a higher exhaust gas temperature (> 700 ° C). (Figure 2).

A reheating furnace consumes in terms of heat from the combustion of natural gas about 350 kWh per ton of steel, and from 25% to 35% of this energy input is still wasted through gaseous effluents, despite measures to improve energy efficiency. It has been assessed that the additional recovery system, that is the energy waste heating system, could recover 50% of this energy loss, corresponding to more than 43 kWh per ton of steel.

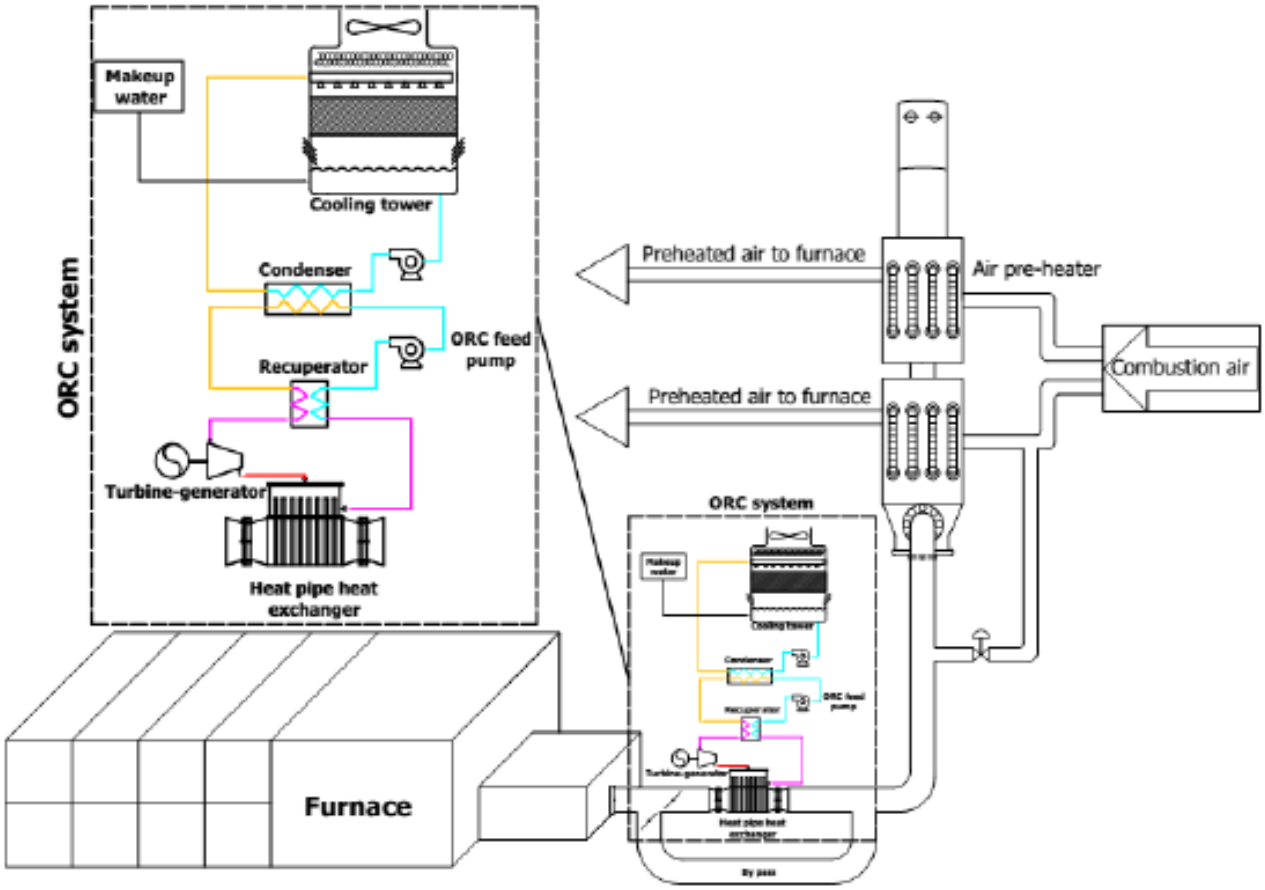

Figure 2. Schematic of waste heat recovery system using ORC connected to a two-phase closed thermosyphon [8]

1.4 Organic Rankine cycle

The Rankine cycle is the fundamental operating cycle of all power plants. This section describes how a Rankine cycle works and what are similarities and differences between a conventional configuration (using steam as a working fluid) and one characterized by the use of an organic compound as a working fluid. This will help to understand why this last type is particularly suitable for the conversion of waste heat into electricity.

1.4.1 Conventional Steam Rankine Cycle (SRC)

In a Rankine cycle a working fluid is continuously evaporated and condensed with the objective of producing mechanical work, which is then converted into electricity by an

alternator. In the simplest configuration, a Rankine cycle is realized by the following thermodynamic transformations:

1-2 Isentropic compression: in the state of saturated liquid, the low-pressure fluid is compressed by a feed pump. Since the specific volume of the liquid in this point has a low value, the pump work is relatively small and often neglectable.

2-3-4 Isobaric evaporation: high pressure liquid is heated in the boiler to the saturation temperature (point 3). During *3-4,* additional provided energy causes evaporation of the liquid reaching the condition of saturated steam. In reality, a further heating process is often required to bring the fluid to superheated steam state. This guarantees a greater vapour quality at the end of the expansion, limiting turbine blades corrosion.

4-5 Isentropic expansion: the steam is in this phase expanded in a turbine producing mechanical work which may be converted in electricity.

5-1 Isobaric condensation: the steam-liquid mixture is condensed at a low pressure (usually below atmospheric pressure) using cooling water.

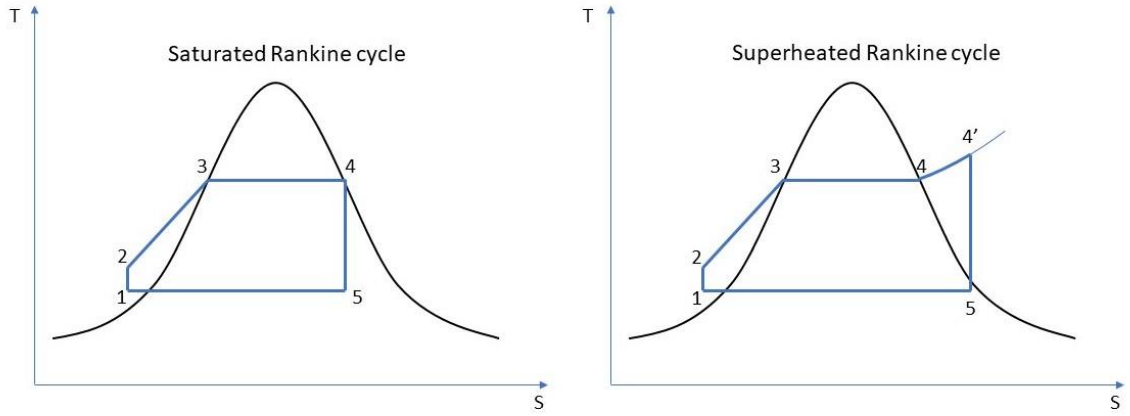

Figure 3. Saturated Rankine cycle and Superheated Rankine cyce

1.4.2 Similarities and differences between SRC and ORC

Regarding thermodynamic transformations, the Organic Rankine Cycle is very similar to a traditional Steam Rankine Cycle. Even this cycle is based on the vaporization of a high-pressure liquid, which is subsequently expanded to a lower pressure level in a turbine,

transforming thermal energy into mechanical work, and then condensed at a low pressure and finally pumped back. Therefore, the Organic Rankine Cycle and the conventional steam power plant are practically composed by the same components:

- A pump
- A boiler
- A work-producing expander (turbine)
- A condenser

While steam power plants can become very complex, with several auxiliary components and different efficiency-improving techniques (e.g. regeneration, cogeneration, reheating processes), the variations of the Organic Rankine Cycles architecture are usually rather limited. The only exception consists in a secondary heat exchanger (recuperator) that can be installed between the pump outlet and the evaporator inlet for pre-heating the liquid improving the efficiency.

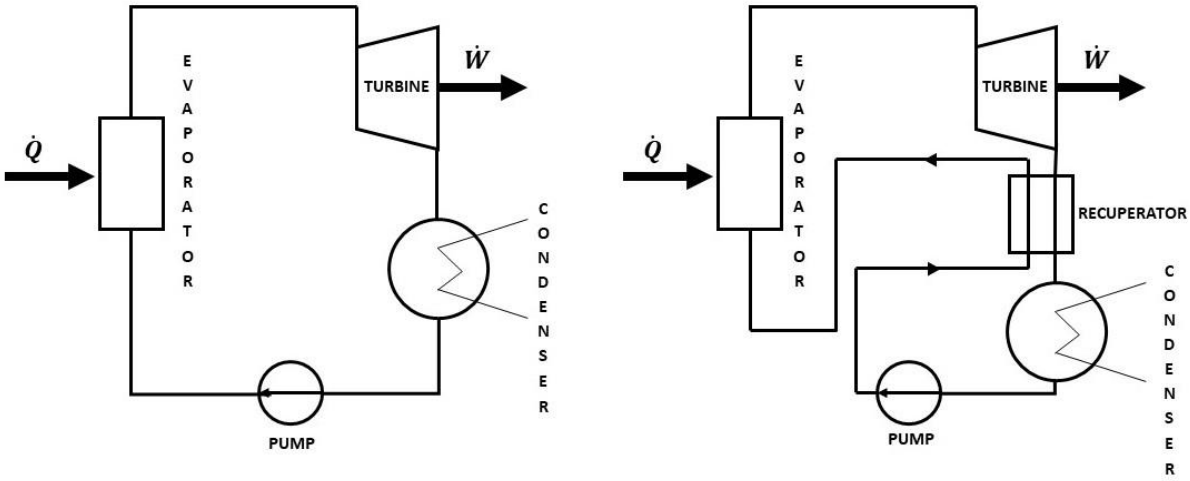

Figure 4. Scheme of an organic Rankine cycle: configuration with and without evaporator

The main difference between an Organic Rankine Cycle and a Steam Rankine Cycle is given by the working fluid, that for the ORC is an organic compound characterized by a low boiling temperature. As a direct result, this allows power generation from lower heat source temperature. This aspect makes the ORC technology more suitable than steam Rankine cycles for converting renewable energy sources whose temperature is lower than that of

traditional fossil fuels [9]. On the other hand, water is a more convenient working fluid considering some of its characteristics, e.g. non-flammability, non-toxicity, chemical stability, non-polluting, low cost. A thermodynamic comparison between water and organic fluids can be made observing the T-s diagram in in Figure 5. It shows the saturation curves of water and other typical organic fluids used in ORC systems.

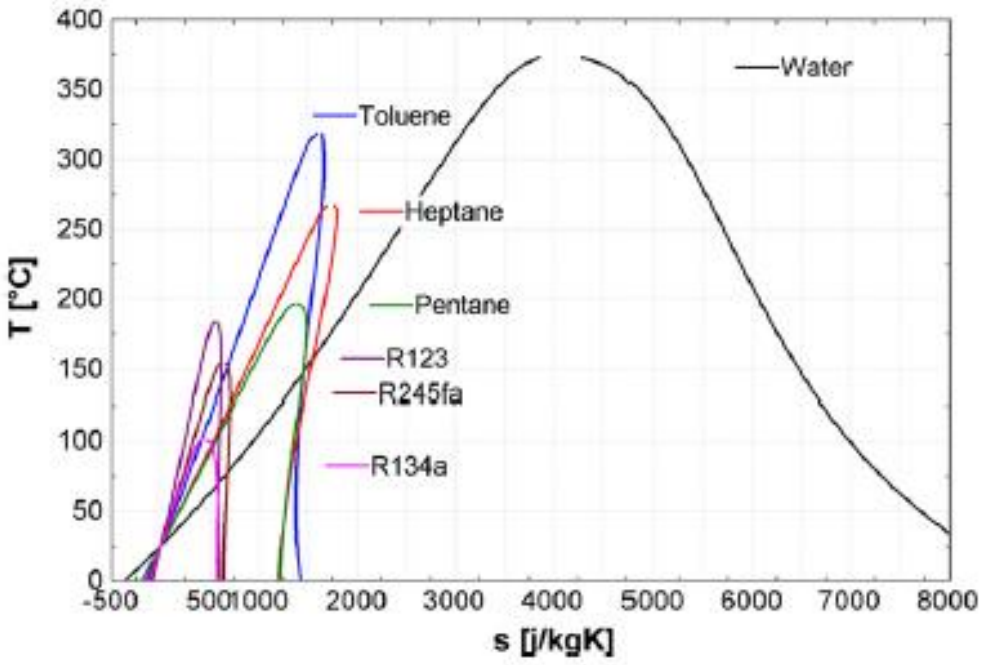

Figure 5. T-s diagram of water and various typical ORC fluids [9]

A first difference can be noticed by focusing on the saturated vapour curves. The slope of the saturated vapour curve presents a negative trend for water, while for organic fluids the curve is substantially vertical. As a result, the organic fluid has the property of remaining superheated at the end of the expansion, eliminating the need of a superheating section in the evaporator. Another advantage deriving from this behaviour is an extension in the turbine lifetime since the absence of condense reduces the risk of corrosion for the blades. A second main difference between the two types of fluids consists in the entropy difference between saturated vapour and saturated liquid, which is much smaller for the organic fluids. Therefore, the latent heat of vaporization is smaller for organic fluids and a higher mass flow rate is required, compared with water, in order to exchange the same thermal power in the evaporator.

Other important differences between the two cycles can be briefly presented [9]:

- Turbine inlet temperature: due to the superheating constraint, in steam Rankine cycle a temperature higher than 450 °C is required, while for ORC the typical working temperature range is within 100 and 300 °C. This leads to lower thermal stresses in the components and lower costs.

- Pressure: similar considerations to those made for the temperature con be also made for pressure. While a steam Rankine cycle often operates over 70 bar, in an ORC pressure normally does not exceed 30 bar, obviously causing less thermal stress for the components.

- Turbine design: in steam power plants, turbines with several stages are usually employed because the enthalpy drop in the expansion phase is very high. The enthalpy drop in ORC systems is much lower and single-stage turbines can be used.

- Efficiency: traditional steam Rankine cycles present a global efficiency usually higher than 30%. Current ORC systems efficiency does not exceed 24% (but with a simpler design in terms of size and number of components)

1.4.3 Organic working fluid selection and ORC most common applications

In the scientific literature, the fluid selection for an Organic Rankine Cycle is covered by a broad range of working fluids. Nevertheless, only a few fluids are used in commercial ORC systems and no single fluid has been identified as optimal yet. One of the reasons are the different hypotheses used by the authors to perform fluid comparisons.

Some authors consider the environmental impact, the flammability, and the toxicity of the working fluid, while other authors do not. Another source of ambiguity is given by the different working conditions assumed, leading to different results even for the same analysed fluid.

It follows that the selection of the working fluid cannot be done a priori, and it has to be integrated into the design process of every ORC system.

In conclusion, some of the main applications for ORC power plants are briefly described in the following section:

- Biomass feeding: by the combustion of biomass, it is possible to produce electricity through a thermodynamic cycle such an ORC. Biomass is widely available in several agricultural and industrial processes and its cost is considerably lower than that of fossil fuels.
- Geothermal energy: with a range of temperatures from a few tens of degrees up to 300°C, geothermal heat sources constitute a valid option for power production by means of ORCs.
- Solar energy: producing electricity by concentrating solar power is a well-proven practice. Some well-establish technologies already perform this task (e.g. parabolic dish, parabolic trough, solar towers) but ORCs are proving to be able to reduce the investment costs at small scale.
- Waste heat recovery from industrial processes: this practice has been already described in this dissertation. Many processes in the manufacturing industry reject heat in the atmosphere causing two types of pollution: direct release of heat, which affects aquatic equilibriums and biodiversity, and pollutants e.g. CO2, NOx, SOx, etc. Therefore, recovering waste heat reduces the pollution and increase the efficiency of the process if the produced electricity is used on-site.

2 Two-phase closed thermosyphon heat exchanger

2.1 Operating principle

The two-phase closed thermosyphon (also called gravity-assisted heat pipe or wickless heat pipe) is a relatively simple device with a great ability to transfer heat. It is vertically oriented and, as shown in figure 6, it consists of a tube where 3 different sections can be distinguished: evaporator, condenser and adiabatic section.

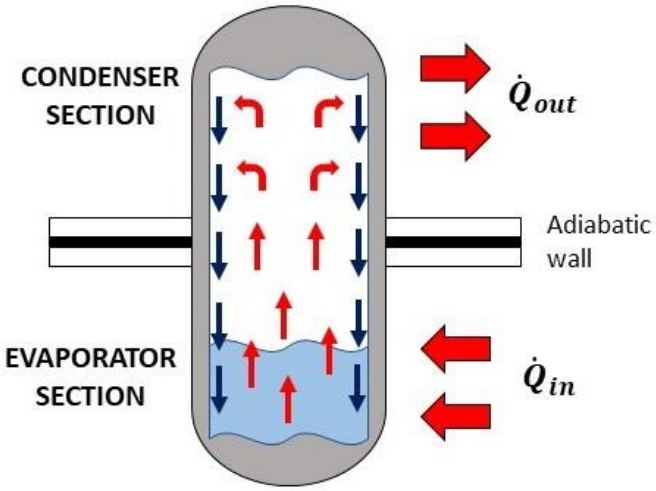

Figure 6. Operating principle of a thermosyphon (or wickless heat pipe)

The operating principle of a two-phase closed thermosyphon is determined by a small amount of working fluid (e.g. water, refrigerant, hydrocarbons, etc.) placed inside a tube. The air and all other gases inside are expelled and then the tube is sealed. The lower end (also called evaporator section) of the tube is in contact with a source of heat, causing the evaporation of the internal liquid. Then, the vapour moves to the cold end (also called condenser section), where it condenses due to the heat release. The condensate is returned to the hot end of the tube by means of gravity. The two sections (evaporator and condenser) of the thermosyphon are separated by an adiabatic wall that avoids direct heat exchanges between the hot and the cold source. In the application examined in this study, the hot source is represented by the exhaust gases of a heating furnace for the steel industry, while the fluid to be heated is the organic compound circulating in the ORC system.

The great efficiency that characterizes the thermosyphon, derives from the phase transformations of the fluid that take place inside of it. The evaporation of a certain quantity of a substance, in fact, even if it takes place at a steady temperature, requires a quantity of heat (latent heat) considerably higher than that needed to only raise its temperature. Using water as an example, the amount of energy required to evaporate 1 gram of liquid is the same amount of energy necessary to raise the temperature of the same gram of 540 °C. As a result, considerable quantities of heat can be transported from end to end with a quasi-isothermal transformation inside the thermosyphon.

A first advantage of this technology is the fact that the amount of heat transported can be many orders of magnitude higher than that of any solid conductor. Secondly, an increase of heat flow at the evaporator section would lead to an increase in the quantity of vaporized liquid without any variation in the operating temperature of the thermosyphon. Another advantage is given by the response time, which for these devices is lower than that provided by other types of heat exchanger. Finally, this type of component does not require any maintenance and the overall structure is very compact.

An example of a heat exchanger consisting of groups of two-phase closed thermosyphons arranged in a casing is shown in Figure 7.

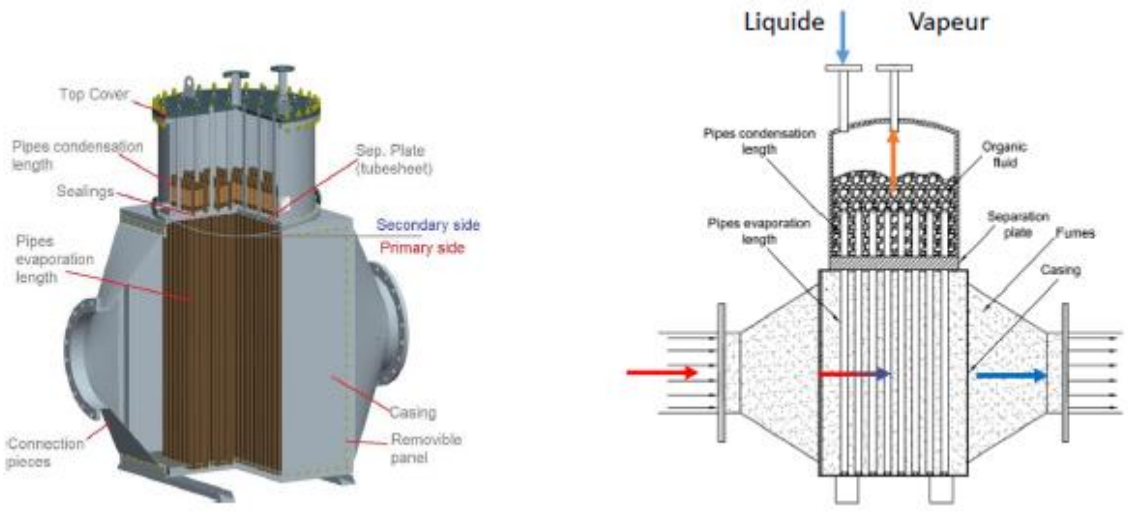

Figure 7. Scheme of a two-phase closed thermosyphon heat exchanger [10]

One limitation of the basic two-phase closed thermosyphon is that, since it exploits the action of gravity to return the condensed fluid to the bottom of the pipe, it is fundamental that the evaporation section is always located at the lowest point of the exchanger [11]. This limit has been resolved by the invention of heat pipes, which work with the same operating principle of a thermosyphon, but their structure is capillary. In these devices, the working fluid is pumped using the only capillary forces generated by the meniscus, which is formed due to evaporation. The result is that heat pipes do not require gravity and can be oriented in any direction. Since their invention, heat pipes have been used in many applications ranging from temperature control of the permafrost layer below the Alaska pipeline to thermal control of optical surfaces in spacecraft, from energy recovery to the cooling of electronic components.

In many countries, the use of thermosyphon heat exchangers is quite new, but other countries, such as China, has applied this technology for decades [12]. Indeed, its compactness, the low maintenance needed, and the low investment and operative costs make thermosyphon heat exchangers an attractive solution when compared to other technologies (e.g. tube-and-shell and plate heat exchangers) [12].

2.2 Theoretical performance of a two-phase closed thermosyphon

The performance calculation of a thermosyphon heat exchanger must be carried out in three steps:

- Calculate the total thermal resistance and determinate the heat flow
- Calculate the operating limits
- Check that the calculated heat flux respects the different operating limits

2.2.1 Total thermal resistance and heat flow

The thermal performance of a two-phase closed thermosyphon can be assumed to be similar to that of a very efficient thermal conductor characterized by a low thermal resistance.

Therefore, the heat flow exchanged in the thermosyphon can be determined by:

$$\dot{Q} = \frac{\Delta T}{R_{tot}} \tag{1}$$

Where

ΔT, $[k]$, is the difference between fumes inlet temperature, $T_{\infty,e}$, and the evaporation temperature of the organic fluid, $T_{\infty,c}$.

R_{tot} $\left[\frac{k}{w}\right]$, is the total thermal resistance of the two-phase closed thermosyphon [13].

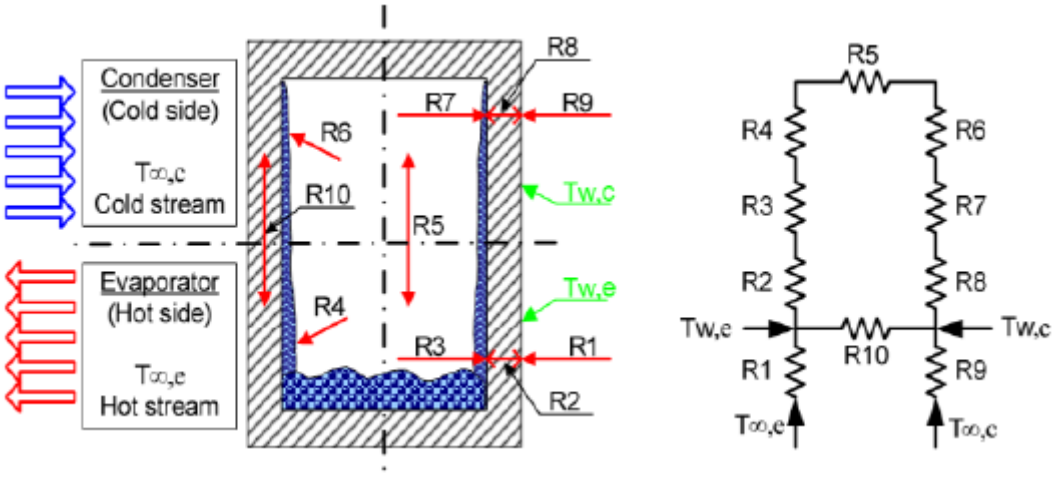

Figure 8. Thermal resistances diagram of a thermosyphon [14]

Where

R_1, R_9 thermal resistances of combined convection and radiation at the outer surface of the evaporator and condenser, respectively.

R_2, R_8 thermal resistances of conduction through the evaporator and condenser walls, respectively.

R_3, R_7 thermal resistances of the boiling and condensation of the working fluid, respectively.

R_4, R_6 thermal resistances at the surface of the liquid-vapour interface in the evaporator and condenser.

R_5 thermal resistance due to vapour pressure drop from evaporator section to condenser section.

R_{10} axial thermal resistance of the thermosyphon wall.

It follows that the total thermal resistance of the thermosyphon can be calculated as [13]:

$$R_{tot} = R_1 + \left(\frac{1}{R_2 + R_3 + R_4 + R_5 + R_6 + R_7 + R_8} + \frac{1}{R_{10}}\right)^{-1} + R_9 \quad (2)$$

Among these resistances, R_{10} assumes a very high value compared to the other ones, so, its inverse in the equation can be neglected.

Consequently, equation (2) becomes:

$$R_{tot} = R_1 + R_2 + R_3 + R_4 + R_5 + R_6 + R_7 + R_8 + R_9 \quad (3)$$

Another simplification can be done considering that resistances R_4, R_5, R_6 are usually small (see page 23 for the calculation) thus neglectable. This leads to the final form of equation (2):

$$R_{tot} = R_1 + R_2 + R_3 + R_7 + R_8 + R_9 \quad (4)$$

In order to have all necessary information for evaluating the thermosyphon performance, the thermal resistances are analysed individually below.

The thermal resistance outside the evaporator section is determined by:

$$R_1 = \frac{1}{h_{eo} A_{eo}} \quad (5)$$

Where

A_{eo} is the outer surface area of the evaporation section, $[m^2]$

h_{eo} is the heat transfer coefficient outside the evaporation section, $\left[\frac{W}{m^2 \cdot K}\right]$

The heat transfer coefficient h_{eo} is the sum of two heat transfer coefficient components, i.e. convective and radiative components:

$$h_{eo} = h_{rad,eo} + h_{conv,eo} \tag{6}$$

The radiative heat transfer component is given by [15]:

$$h_{rad,eo} = 5.67 \cdot 10^{-8} \frac{\varepsilon_f T_f^4 - \alpha_f T_w^4}{T_f - T_w} \tag{7}$$

Where

ε_f is fumes emissivity, [-], given by:

$$\varepsilon_f = \frac{a_0 + a_1[log_{10}(pL_M \frac{T_w}{T_f})] + a_2[log_{10}(pL_M \frac{T_w}{T_f})]^2 + a_3\left[log_{10}\left(pL_M \frac{T_w}{T_f}\right)\right]^3}{T_{\mathrm{w}}} \tag{8}$$

$$p = p_{CO_2} + p_{H_2O} \tag{9}$$

$$L_M = 1.08 \frac{S_T S_L - 0.785 d_o^2}{d_o} \tag{10}$$

α_f is fumes absorptivity, [-], given by:

$$\alpha_f = 0.5 \left(\frac{T_w}{T_f}\right) \cdot \varepsilon_f \left(T_{w,} L_M \frac{T_w}{T_f}\right) \tag{11}$$

T_f is fumes temperature, [K]

T_w is wall temperature, [K]

p_{CO_2} is the partial pressure of CO_2, [atm]

p_{H_2O} is the partial pressure of water vapour, [atm]

d_o is the thermosyphon outer diameter, [m]

S_T is the transverse tube pitch, [m]

S_L is the longitudinal tube pitch, [m]

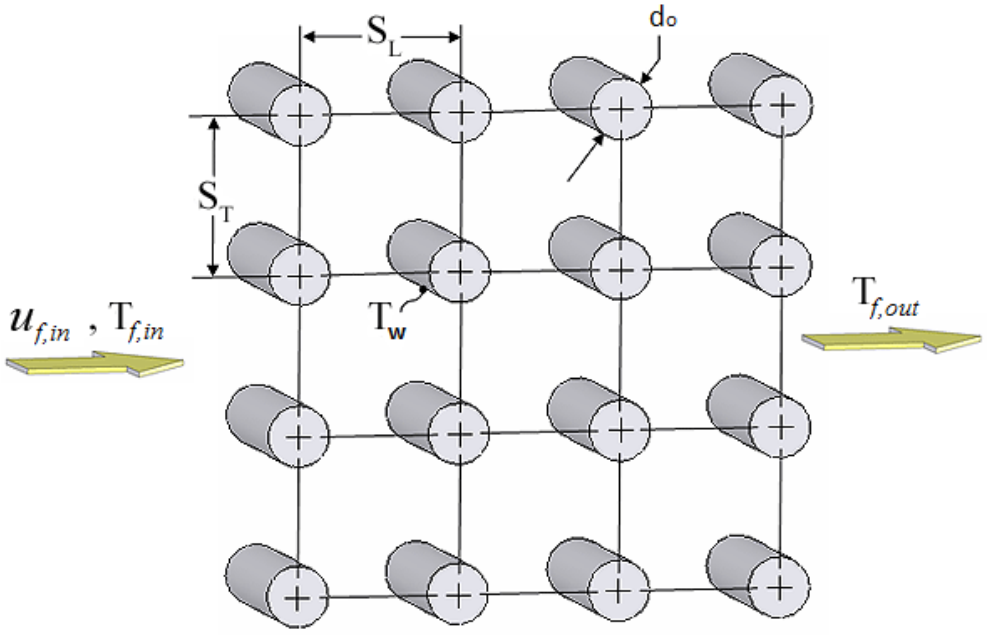

Figure 9. External flow inline bank [16]

The convective heat transfer coefficient can be calculated as follow:

$$h_{conv,eo} = Nu\frac{\lambda_f}{d_o} \tag{12}$$

With

The Nusselt number given by the Zukauskas correlation [17]:

$$\mathrm{Nu} = \mathrm{C} \cdot Re^{m} \cdot Pr^{0,36} \cdot \left(\frac{Pr}{Pr_w}\right)^{0,25} \tag{13}$$

The Reynolds number given by:

$$\mathrm{Re} = \frac{\rho \cdot V_{max} \cdot d_o}{\mu_f} \tag{14}$$

With V_{max} the maximum velocity of fumes inside the heat exchanger, given by:

$$V_{max} = \frac{S_T}{S_T - d_o} \cdot u_{f,in} \tag{15}$$

Where

λ_f is the thermal conductivity of fumes, $\left[\frac{W}{m \cdot K}\right]$

C is a coefficient depending upon Reynolds number value, [-]

m is an exponential coefficient depending upon Reynolds number value, [-]

Pr is Prandtl number at bulk temperature, [-]

Pr_w is Prandtl number at thermosyphon wall temperature, [-]

μ_f is viscosity of fumes $[Pa \cdot s]$

$u_{f,in}$ is the velocity of fumes at the inlet of the heat exchanger $\left[\frac{m}{s}\right]$

The thermal resistance outside the condenser section is determined by:

$$R_9 = \frac{1}{h_{co} A_{co}} \tag{16}$$

With the heat transfer coefficient outside the condenser section, h_{co}, determined, using the Cooper correlation [18], as the heat transfer coefficient of pool boiling of the organic fluid:

$$h_{co} = 55 \cdot MM^{-0,5} \cdot q_{flux}^{0,67} \cdot p_r^{0,12-0,2\log_{10} R_p} \cdot [-\log_{10}(p_r)]^{-0,55} \tag{17}$$

Where

A_{co} is the outer surface area of the condensation section, $[m^2]$

MM is the molecular weight, $\left[\frac{kg}{kmol}\right]$

q_{flux} is heat flux density, $\left[\frac{W}{m^2}\right]$

p_r is reduced pressure defined as $p_r = \frac{P_{sat}}{P_{cr}}$, [-]

R_p is the wall surface roughness , [-]

The thermal resistances of conduction through the evaporator and condenser walls of the thermosyphons are given by, respectively:

$$R_2 = \frac{\ln\left(\frac{d_o}{d_i}\right)}{2 \cdot \pi \cdot l_e \cdot \lambda_w} \tag{18}$$

$$R_8 = \frac{\ln\left(\frac{d_o}{d_i}\right)}{2 \cdot \pi \cdot l_c \cdot \lambda_w} \tag{19}$$

Where

d_i is the thermosyphon inner diameter, [m]

l_e is the evaporation section length, [m]

l_c is the condensation section length, [m]

λ_w is the wall material thermal conductivity, $\left[\frac{W}{m \cdot K}\right]$

The thermal resistance R_3 depends on two boiling mechanisms taking place in the evaporation side, i.e. pool boiling and film boiling. In the first case, boiling occurs through the nucleation of bubbles at the liquid-wall contact surface. During this process the motion of the liquid is caused by the bubbles themselves and speeds are to be considered low. The second case occurs when the temperature of the wall increases and reaches a critical point, beyond which the steam produced forms an insulating layer over the surface and, consequently, the heat transfer coefficient is deteriorated.

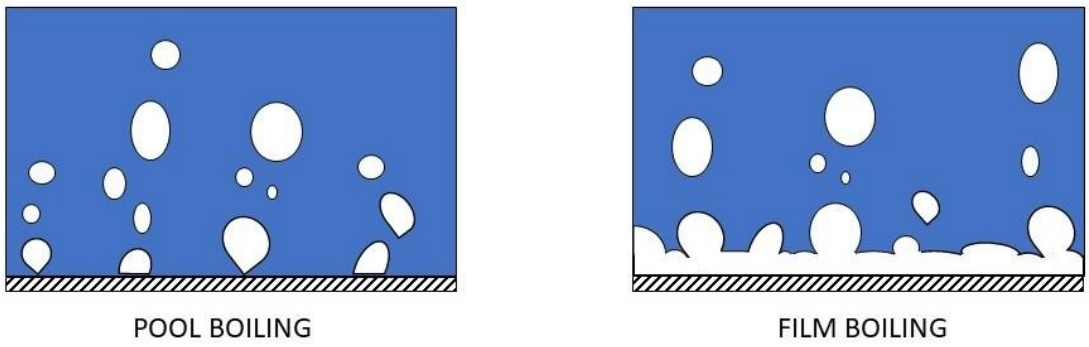

Figure 10. Schematic of the phenomena of pool boiling and film boiling

Resistance R_3 can be determined as follow:

$$\begin{cases} R_3 = R_{3p} & R_{3p} < R_{3f} \\ R_3 = R_{3p}F + R_{3f}(1-F) & R_{3p} \geq R_{3f} \end{cases} \quad (20)$$

With

F, the rate of filling of liquid inside the evaporator, [-]

$$\mathrm{F} = \frac{V_l}{A \cdot l_e} \tag{21}$$

R_{3p} is the thermal resistance due to pool boiling phenomenon:

$$R_{3p} = \frac{1}{\Phi_3 \cdot g^{0.2} \cdot \dot{Q}^{0.4} \cdot (\pi \cdot d_i \cdot l_e)^{0.6}} \tag{22}$$

With

$$\Phi_3 = \frac{0{,}32 \cdot \rho_l^{0{,}65} \cdot \lambda_l^{0{,}3} \cdot cp_l^{0{,}7}}{\rho_v^{0{,}25} \cdot \Delta h_{lv}^{0{,}4} \cdot \mu_l^{0{,}1}} \cdot \left(\frac{P_{sat}}{P_{atm}}\right)^{0{,}23} \tag{23}$$

R_{3f} is the thermal resistance due to film boiling phenomenon:

$$R_{3f} = \frac{0.235 \cdot \dot{Q}}{d_i^{4/3} \cdot g^{1/3} \cdot l_e \cdot \mathrm{FOM}_t^{4/3}} \tag{24}$$

Where

V_l is the initial volume of liquid inside the evaporator $[m^3]$

A is the internal passage section of the thermosyphon $[m^2]$

g is gravitational acceleration $\left[\frac{m}{s^2}\right]$

ρ_v and ρ_l are vapour and liquid density, respectively, $\left[\frac{kg}{m^3}\right]$

λ_l is the thermosyphon working fluid thermal conductivity, $\left[\frac{W}{m \cdot K}\right]$

cp_l is the thermosyphon working fluid specific heat capacity $\left[\frac{J}{kgK}\right]$

Δh_{lv} is the latent heat of the thermosyphon working fluid $\left[\frac{J}{kg}\right]$

μ_l is the thermosyphon working fluid viscosity $[Pa \cdot s]$

P_{sat} is the thermosyphon working fluid saturation pressure $[Pa]$

P_{atm} is the atmospheric pressure $[Pa]$

FOM_t is the figure of merit of the thermosyphon working fluid $\left[\frac{kg}{K^{3/4} \cdot s^{5/2}}\right]$

The thermal resistance R_7 is given by:

$$\begin{cases} R_7 = 191 \cdot R_{7f} \cdot Re_f^{-0,733} & Re_f > 1300 \\ R_7 = R_{7f} & 50 < Re_f < 1300 \end{cases} \tag{25}$$

$$R_{7f} = \frac{0.235 \cdot \dot{Q}}{d_i^{4/3} \cdot g^{1/3} \cdot l_c \cdot \mathrm{FOM}_t^{4/3}} \tag{26}$$

For completeness, the equations for calculating the thermal resistances considered neglectable, are provided below:

$$R_4 = \frac{R \cdot T_{ve}^2 \cdot (2 \cdot \pi \cdot R \cdot T_{ve})^{0,5}}{\Delta h_{lv,e}^2 \cdot P_{ve} \cdot A_{eo}} \tag{27}$$

$$R_6 = \frac{R \cdot T_{vc}^2 \cdot (2 \cdot \pi \cdot R \cdot T_{vc})^{0,5}}{\Delta h_{lv,c}^2 \cdot P_{vc} \cdot A_{co}} \tag{28}$$

$$R_5 = \frac{T_{ve} - T_{vc}}{\dot{Q}} \tag{29}$$

Where

R is the constant for ideal gas, R=8314 $\left[\frac{J}{kmol \cdot K}\right]$

T_{ve} is the temperature of the thermosyphon working fluid vapour in the evaporation section [K]

T_{vc} is the temperature of the thermosyphon working fluid vapour in the condensation section [K]

$\Delta h_{lv,e}$ is the latent heat of the thermosyphon working fluid at T_{ve} $\left[\frac{J}{kg}\right]$

$\Delta h_{lv,c}$ is the latent heat of the thermosyphon working fluid at T_{vc} $\left[\frac{J}{kg}\right]$

P_{ve} is the thermosyphon working fluid vapour pressure in the evaporation section $[Pa]$

P_{vc} is the thermosyphon working fluid vapour pressure in the condensation section $[Pa]$

Thermal resistance R_{10} due to the thermosyphon wall in the axial direction (usually very large and for this reason its contribution in the equation (2) can be neglected) can be calculated as:

$$R_{10} = \frac{0{,}5 \cdot l_e + l_a + 0{,}5 \cdot l_c}{A_x \cdot \lambda_w} \tag{30}$$

Where

A_x is the cross-sectional area of the thermosyphon shell $[m^2]$

l_a is the thickness of the adiabatic wall between the evaporation and condensation section [m]

2.2.2 Operating limits

All useful equations to calculate the performance of a thermosyphon have been presented in the previous paragraph. The next step, as announced above is to determine all the operating limits that will impose the final thermal flow. In the case of the two-phase closed thermosyphon, five most important occurring phenomena are: Viscous Limit (or Vapour Pressure Limit), Sonic Limit, Dry-out Limit, Boiling limit (or Burnout Limit) and Entrainment Limit (or Counter-Current Flow Limit).

Viscous Limit (Vapour Pressure Limit)

This condition can occur when the thermosyphon operates at temperatures below its normal operating range, such as during start-up phase. As a consequence, viscous forces may be dominant for the vapour moving flow down the thermosyphon and the heat transfer may be limited. The maximum rate of heat transfer imposed by this limit is given by:

$$\dot{Q}_{max,visc} = \frac{d_i^2 \cdot \Delta h_{lv} \cdot p_v \cdot \rho_v}{64 \cdot \mu_v \cdot l_{eff}} \tag{31}$$

Where

μ_v is the vapour dynamic viscosity $[Pa \cdot s]$

$l_{eff} = \frac{l_e}{2} + l_a + \frac{l_c}{2}$ is the effective thermosyphon length [m]

Sonic Limit

At low operating temperature (e.g. start-up condition), when the vapour pressure at the condenser section in low as well, the increasing heat flow rate implies an increase of the vapour velocity. If vapour velocity reaches the speed of sound the vapour flow becomes "choked". When the sonic limit is reached, further increases in the heat transfer rate can be realized only when the evaporator temperature increases. To avoid choked flow condition the recommended heat flow rate is given by:

$$\dot{Q}_{max,sonic} = 0.474 \cdot A \cdot \Delta h_{lv} \cdot (p_v \cdot \rho_v)^{1/2} \tag{32}$$

Dry-out Limit

Dry-out condition take place when most of the falling condensate liquid has evaporated before reaching the pool, leaving dry patches with only few rivulets of liquid returning to the bottom of the pipe. This phenomenon occurs when the volume of the liquid is not sufficient to guarantee the presence of a film of liquid over the entire inner surface of the pipe. Usually this situation can be avoided by selecting a fill ratio for the thermosyphon (defined by (21)) included between 0.4 and 0.6 [19].

Boiling Limit

Boiling limit (or burnout limit) takes into consideration the risk that a stable film of vapour could be formed between the liquid and the hot wall of the thermosyphon in the evaporation side [13]. The critical boiling heat flow can be determined by:

$$\dot{Q}_{max,boiling} = 0{,}12 \cdot A_{ie} \cdot (\rho_v)^{0{,}5}[\sigma \cdot g \cdot (\rho_l - \rho_v)]^{0{,}25} \qquad (33)$$

Where

A_{ie} is the inner surface of the evaporation section $[m^2]$

σ is the surface tension of the liquid $\left[\frac{N}{m}\right]$

Entrainment Limit

Inside the thermosyphon, vapour and liquid circulate in a counter current way. Because of the high speeds reached by the vapour, it could drag some of the liquid, preventing this last to return to the evaporation section. The counter-current limit (or entrainment limit) avoid this phenomenon by imposing a maximum value for the heat flow exchanged in the thermosyphon [13]:

$$\dot{Q}_{max,CCFL} = f_1 \cdot f_2 \cdot f_3 \cdot A \cdot \Delta h_{lv} \cdot (\rho_v)^{0{,}5}[g \cdot (\rho_l - \rho_v)]^{0{,}25} \qquad (34)$$

Where

f_1 is a function of the Bond number, which is defined as:

$$Bo = d_o \left[\frac{g \cdot (\rho_l - \rho_v)}{\sigma}\right]^{0,5} \tag{35}$$

f_2 is a function of the dimensionless pressure parameter K_p, defined as:

$$K_p = \frac{p_v}{[g \cdot \sigma \cdot (\rho_l - \rho_v)]^{0,5}} \tag{36}$$

$$\begin{cases} f_2 = K_p^{-0,17} & K_p \leq 4 \cdot 10^4 \\ f_2 = 0{,}165 & K_p > 4 \cdot 10^4 \end{cases} \tag{37}$$

f_3 is a factor in function of the inclination of the thermosyphon pipes. When the pipes are vertical, it can be imposed equal to 1.

The operating limits are represented in the following qualitative graph:

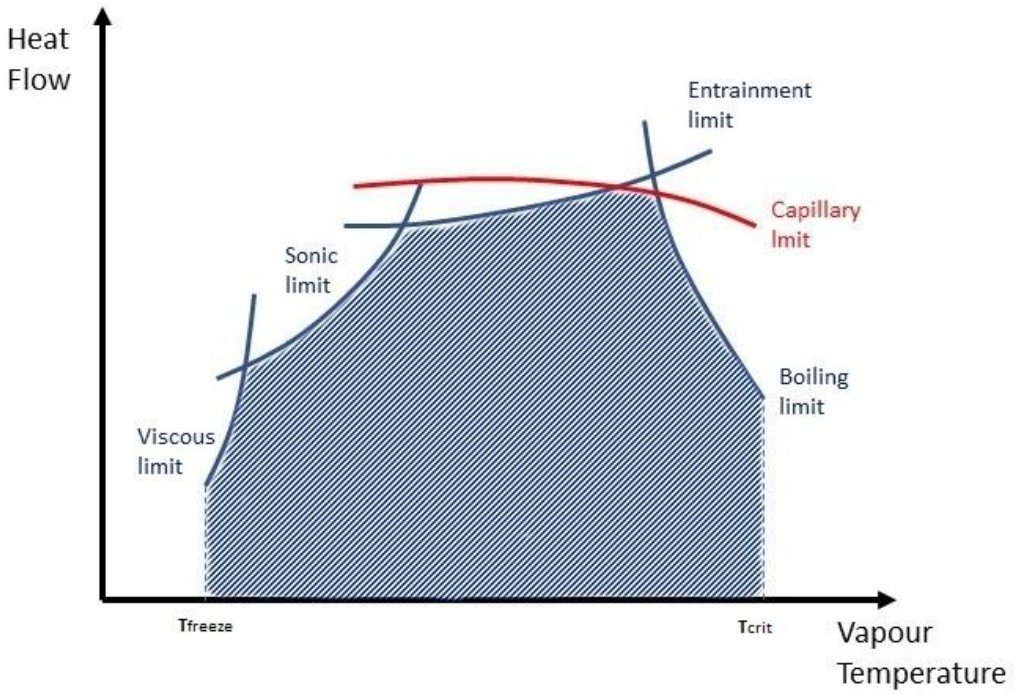

Figure 11. Operating limits for a two-phase closed thermosyphon

Capillary limit is typical for traditional heat pipes (which are characterized by smaller diameters) and for this reason has been neglected.

In lights of these considerations, the operating limit for a thermosyphon must be chosen as the minimum value between the different limits that have been described above. Furthermore, it is advisable to size the thermosyphon so that its nominal working point corresponds to a heat flow equal to 50% of the critical heat flow just calculated. As a result, the maximum heat transfer rate can be defined as:

$$\dot{Q}_{max} = 0.5 \cdot MIN(\dot{Q}_{max,boiling}, \dot{Q}_{max,CCFL}, \dot{Q}_{max,visc}, \dot{Q}_{max,sonic}) \qquad (38)$$

2.2.3 Procedure for performance calculation

The procedure for calculating the performance of the two-phase thermosyphon, through the thermal resistances and the operating limits previously introduced, is summarized in the following conceptual diagram:

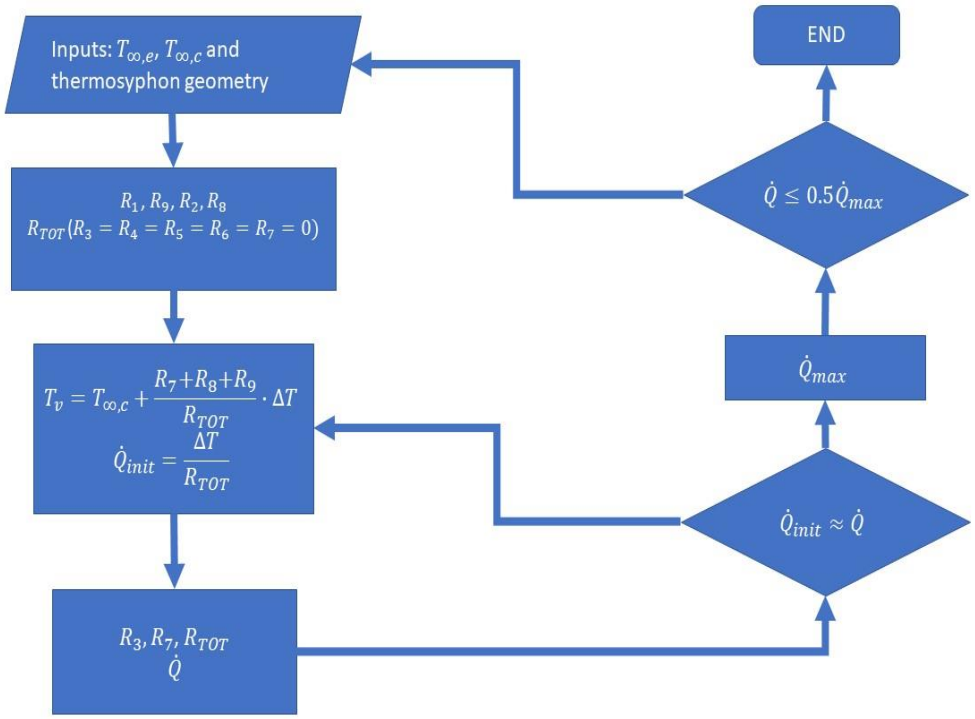

Figure 12. Procedure for the calculation of the thermal power exchanged in a two-phase closed thermosyphon.

Assuming to know as input the geometry of the thermosyphon and the inlet temperature of both the fumes and the organic fluid, it is possible to calculate the resistances R_1, R_9, R_2, R_8.

As explained in section 2.2.1, the resistances 4,5,6 may be neglected. In this phase, also resistances 3 and 7 will be imposed equal to zero since they depend on the heat flux. Thanks to these assumptions it is possible proceed with the calculation of the global thermal resistance (R_{TOT}), the vapour temperature inside the thermosyphon (T_v) and a preliminary value for the heat flow $(\dot{Q}_{init})$. Then follows the calculation of the resistances 3 and 7 which allow to obtain a new value for the heat flow $(\dot{Q})$. If the value of the latter is too different from that of the preliminary heat flow, it is necessary to restart the procedure using $\dot{Q}$ to calculate a new value for R_{TOT} and T_v. If instead, $\dot{Q}_{init}$ and $\dot{Q}$ are comparable it means that thermal resistances 3 and 7 are neglectable and it is possible proceed evaluating the operating limits. If the constraint imposed by the operating limits is not satisfied, it is necessary to review the parameters of thermosyphon geometry or the working temperatures and repeat the procedure.

2.3 Two-phase thermosyphon working fluid and material

As evinced by equations used for the performance calculation of a thermosyphon, the selection of the working fluid plays a fundamental role. Several aspects must be considered such as: range of working temperature, chemical compatibility between the thermosyphon material and the working fluid, vapour pressure, stability, toxicity etc. A common method, in the field of thermosyphon heat exchangers, for selecting working fluids is by means of the figure of merit (FOM_t). This parameter, which has dimension $\frac{kg}{K^{3/4} \cdot s^{5/2}}$ is defined as follow [11]:

$$FOM_t = \left(\frac{\rho_l^2 \lambda_l^3 \Delta h_{lv}}{\mu_l} \right)^{1/4} \tag{39}$$

Although this number has no physical meaning, it enables to compare the performance of different suitable fluids for this application. Straightforwardly, the higher the figure of merit

of the fluid is, the higher will be the performance of the thermosyphon. The thermo-physical properties that compose the figure of merit are dependent on the temperature. It follows that, firstly, it is necessary to establish the range of working temperature. In order to do so, it must be considered that the heat transfer coefficient on the fumes side is much lower than the coefficient on the organic working fluid side. As a result, the thermal resistance due to convective and radiative effects are very different between the two extreme sections, with $R_1 > R_9$, it follows that the temperature of the thermosyphon is closer to the temperature of the ORC working fluid than fumes temperature. Based on this statement, a plausible temperature range for the working fluid inside the thermosyphon can be set within 150-300 °C.

The results obtained comparing different common fluids are shown in Figure 13.

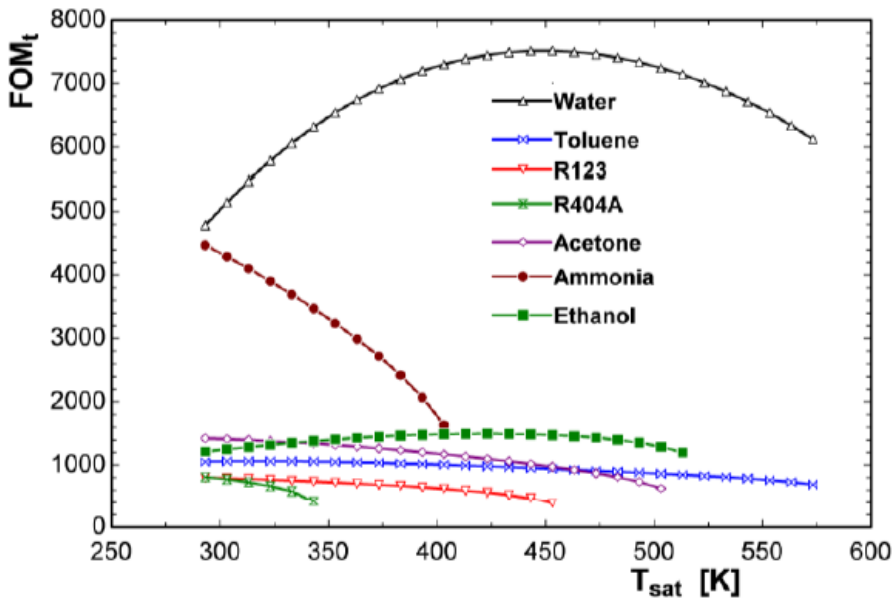

Figure 13. Figure of merit for different two-phase closed thermosyphon working fluid [8].

In this temperature range, has emerged that water presents a relative high figure of merit compared to the other analysed fluids. It seems to be logic to choose this fluid considering other advantages such as high latent heat, stability, no-toxicity, availability, low price, familiarity etc. The main concern about water is the vapour pressure, which can increase significantly with the temperature. This requires that the casing material of the thermosyphon must be selected so that it can endure the high vapour pressure [12]. Thus, the selection of

tube material is a very important parameter as well. Not only for the mechanical strength it must ensure, but it has also to be compatible with the working fluid and the environment. The fluid and the tube material should not react chemically, to avoid the generation of non-condensable gases, which can affect the thermosyphon performance. The non-condensable gases in fact, are pushed to the upper end of the pipe reducing the volume of the condensation region and causing a drop in the performance of the device.

Table 1 shows a list of compatibility between common tube materials and working fluids.

Table 1. Working fluid and tube material compatibility list [12].

Fluid	Recommended	Not recommended
Ammonia	Aluminium, Steel, Stainless steel, Nickel	Copper
Acetone	Copper, Silica, Aluminium, Stainless steel	
Methanol	Copper, Stainless steel, Carbon steel, Silica	Aluminium
Mercury	Stainless steel	Nickel, Inconel, Titanium, Niobium
Water	Copper, Monel, Silica, Nickel, Stainless steel, Carbon steel	Aluminium, Inconel
Naphthalene	Carbon steel, Stainless steel	
Potassium	Stainless steel, Inconel	Titanium
Sodium	Stainless steel, Inconel	Titanium
Silver	Tungsten, Tantalum	Rhenium

3 Experimental case study

The aim of the experimental investigation is to test a heat exchanger prototype which present similarities with a thermosyphon. The thermal power of the prototype is smaller (24 kW) than the one normally available in a real application (see section 1.3), to be operated easily in a lab. This experimental campaign will help to understand the physics related to the thermosyphon technology. First, the performance will be assessed in terms of efficiency and pressure drop. Also, the experimental database will be useful to understand the technical limitations of such a heat exchanger (counter current and boiling limitations, see section 2.2.2). Moreover, it will be possible to evaluate the accuracy of the model and to validate the assumptions that have been made. The validation of the model will allow the extrapolation to larger power and to performs evaluation of the technical and economic feasibility of some given study case from industry.

This chapter describes the test bench, which have been assembled at the Thermodynamic Laboratory of the University of Liège, illustrating first, the individual components and the data acquisition system and eventually, the results of the experimental campaign.

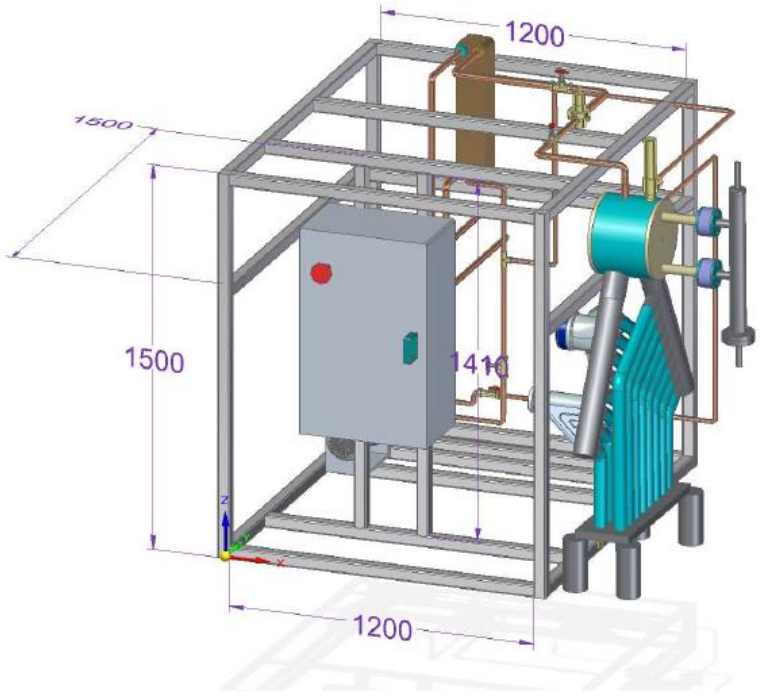

Figure 14. 3D schematic of the test bench.

3.1 Global architecture

A hydraulic scheme of the test bench is outlined in Figure 15 with all the components shown: pump, evaporator, expansion valve, condenser, valves and sensors.

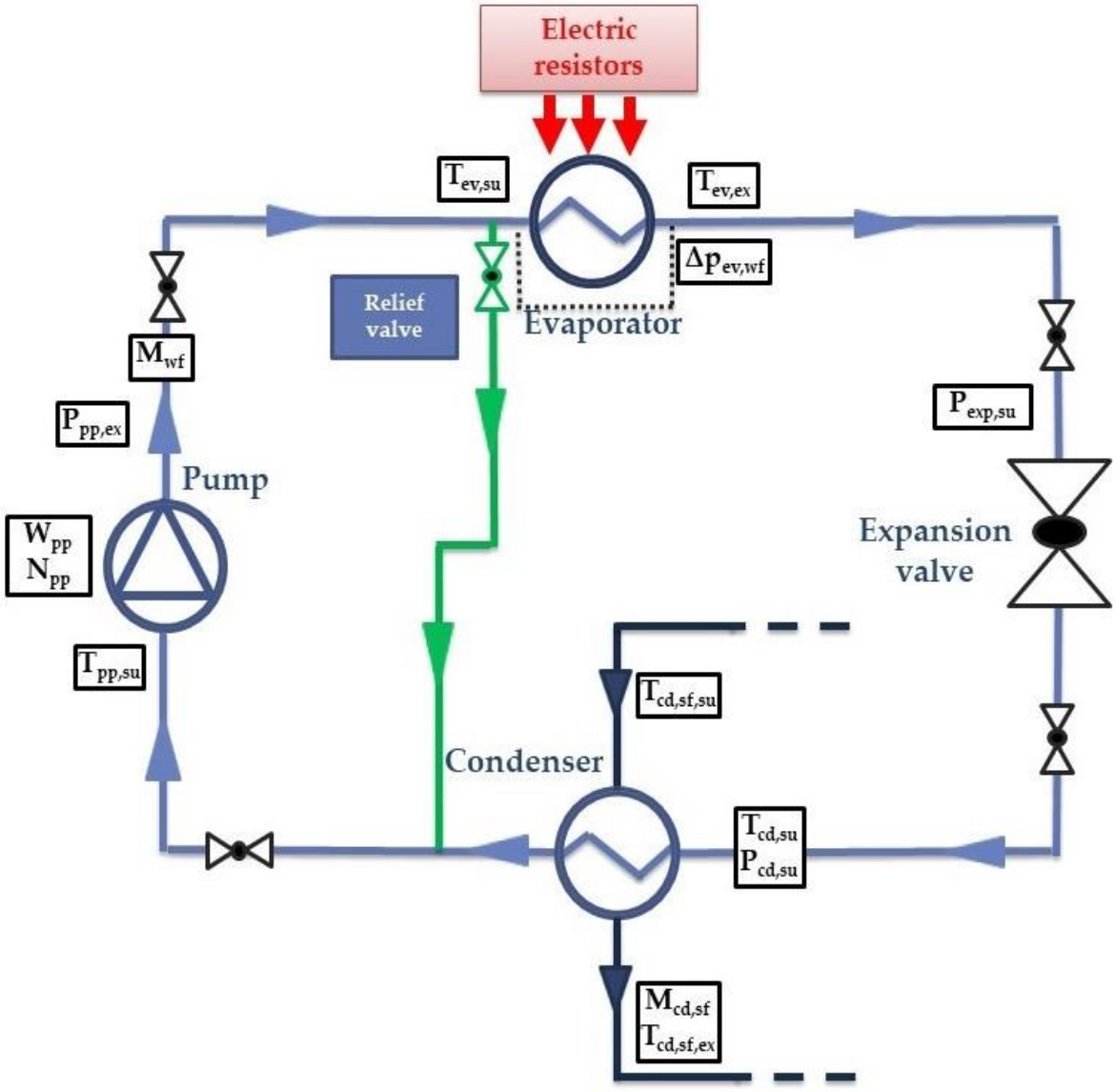

Figure 15. Hydraulic scheme of the test bench.

In the primary circuit, represented in light blue, flows the organic working fluid (R245fa). The dark blue loop symbolizes tap water, used by the condenser for the cooling process. At last, the green line shows a secondary piping that, if necessary, can be used for releasing pressure through a relief valve.

The system is a scale-lab reproduction and a few simplifications in the conventional ORC architecture have been necessary. Since the main objective of the experimental investigation is not to produce electricity through the ORC unit but, it is to focus on the evaporator and collect useful data about its interaction with the organic compound, the expansion machine (turbine) has been replaced by an expansion valve that can provide the necessary pressure drop. The expansion machine is still the most critical component in the scope of Organic Rankine cycles; including it would have complicated the analysis without bringing benefits for the purpose of the project.

The second main variation consists in the heat source of the system. The simplest method to simulate in laboratory the heat flow coming from the exhaust gas, is by using electric resistors placed at the bottom of the evaporator, providing a global power of 24 kW.

Important simplifications have been also made in the geometry of the evaporator, which will be described together with the other components in the following part.

3.2 Components

3.2.1 Pump

The pump installed is a three piston-diaphragm pump developed by Wanner Hydra-Cell (model VB-G03XKSEHFEHJ) coupled to an inverter for controlling the rotational speed. In its simplest form, a piston-diaphragm pump consists of a piston acting on a membrane (in this case made of EPDM) and two check valves, one at the suction and one at the outlet of the pump. When the piston moves backwards a depression is created and the fluid is sucked into the chamber of the pump. Then, when the piston moves forward, the pressure inside the chamber increase and the check valve at the outlet opens, discharging the fluid. At the same time the check valve at the suction closes preventing the fluid to going back. The mechanism is illustrated in figure 16.

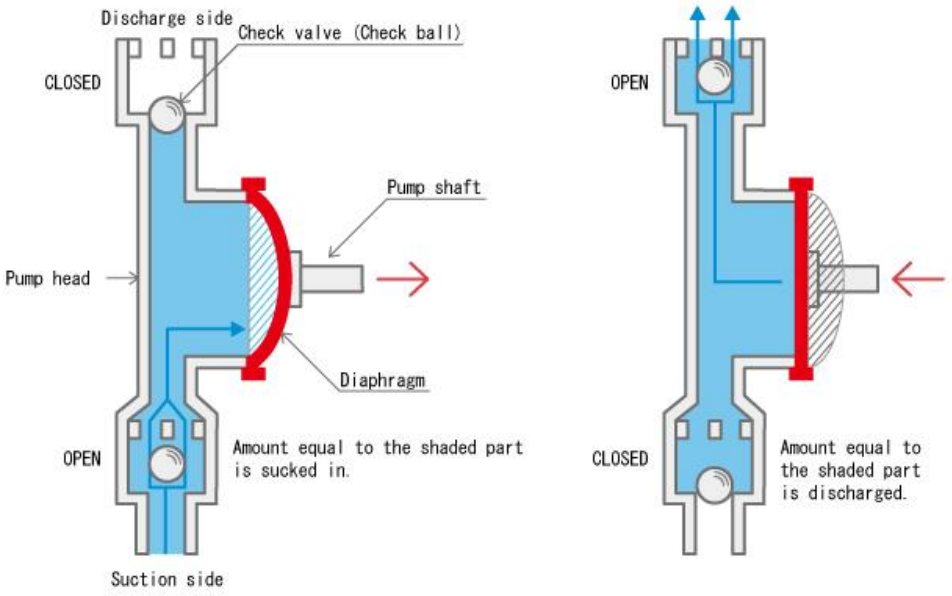

Figure 16. Working principle of a diaphragm pump [20].

This type of pump is conventionally used in small-scale applications because of its ability to handle high pressure drops and low mass flow rate with decent efficiency. The following table summarizes the capacities of the pump installed.

Table 2. Pump technical data.

Parameter	Value	U.o.M.
Maximum inlet pressure	17	bar
Maximum discharge pressure	103	bar
Maximum operating temperature	121	°C
Maximum flow rate	11.7	l/min

3.2.2 Condenser

The condenser used is a counter-current plate heat exchanger developed by SWEP (model B80Hx40/1P-SC-S 4x1 1/4"&28U). In the pressure range usually encountered in ORC applications (20-30 bar), this technology guarantees high efficiency and compactness at a low cost if compared to a tube and shell heat exchanger. A plate heat exchanger consists of

a series of parallel metal plates that create channels for fluids to flow between them. Such flow through the alternating channels, is permitted by inlet and outlet holes located at the corners of the plates. As a result, each plate is always in contact on one side with the hot fluid and the other with the cold fluid, providing a large exchange surface with a very compact layout.

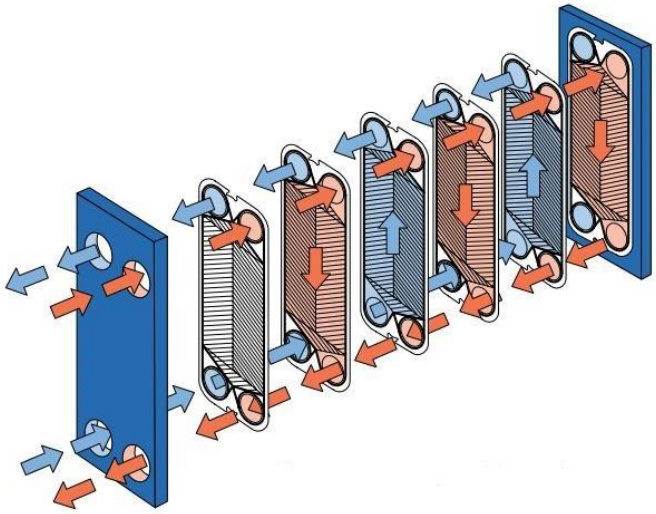

Figure 17. Working principle of a plate heat exchanger [21].

Table 3 summarizes the specifications of the model installed on the test rig.

Table 3. Plate Condenser technical data.

	Parameter	Side 1 (R245fa)	Side 2 (Water)	U.o.M.
Nominal Duty Requirements	Heat load	24,2	24,2	kW
	Inlet temperature	93,05	15	°C
	Outlet temperature	20	30	°C
	Condensation temperature	30	-	°C
	Flow rate	0,09154	1,392	kg/s
Plate heat exchanger	Total heat transfer area	2,28	2,28	m^2
	Heat flux	10,6	10,6	kW/m^2
	Mean temperature difference	9,97	9,97	K
	Pressure drop	7,73	2,98	kPa
	Operating pressure-outlet	171	-	kPa
	Number of channels	19	20	-
	Number of plates	40	40	-
	Inlet velocity	10,7	0,452	m/s

3.2.3 Evaporator

The evaporator installed, which is shown in figure 18, is a prototype which presents similarities with a two-phase closed thermosyphon heat exchanger.

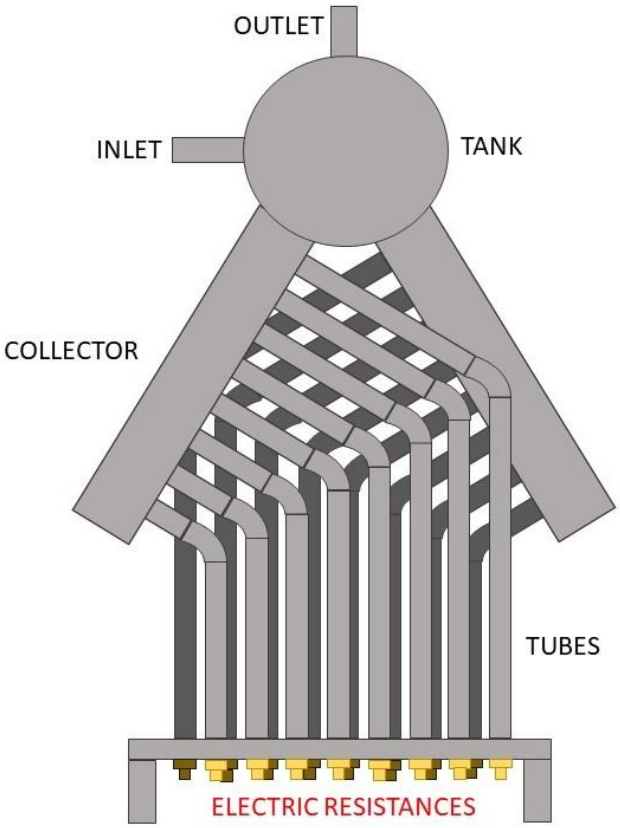

Figure 18. Scheme of the evaporator prototype

In the prototype geometry, three main parts can be identified: at the top, there is the tank (through which the working fluid is received and expelled), then, the two oblique collectors and finally the 16 tubes, inside which the electric resistances are arranged. The global thermal power (24 kW) is provided by 16 electric resistances of 1500 W each. The component is completely built in stainless steel to prevent corrosive phenomena.

As previously introduced, the objective of the study is to better understand the physics which the thermosyphon is based on and, above all, focusing on the convective motion of the fluid inside the tubes. This phenomenon is certainly the most critical aspect for a thermosyphon and for this reason, it is of great interest to evaluate the behavior of such technology when it is applied to an ORC unit. In other words, the expectations for this experimental analysis are to succeed in creating an efficient convective heat exchange inside the device, in order to feed the ORC unit with a fluid at the right energy level.
The result of the previous considerations led to make important simplifications in the geometry, as well as in the operation of the evaporator. The prototype, in fact, has been built to operate with a single fluid instead of two different fluids as required for a traditional two-

phase thermosyphon. The organic working fluid will, therefore, fill both a portion of the upper tank, as normally expected for a thermosyphon, and collectors and tubes, inside which the evaporation process will occur.

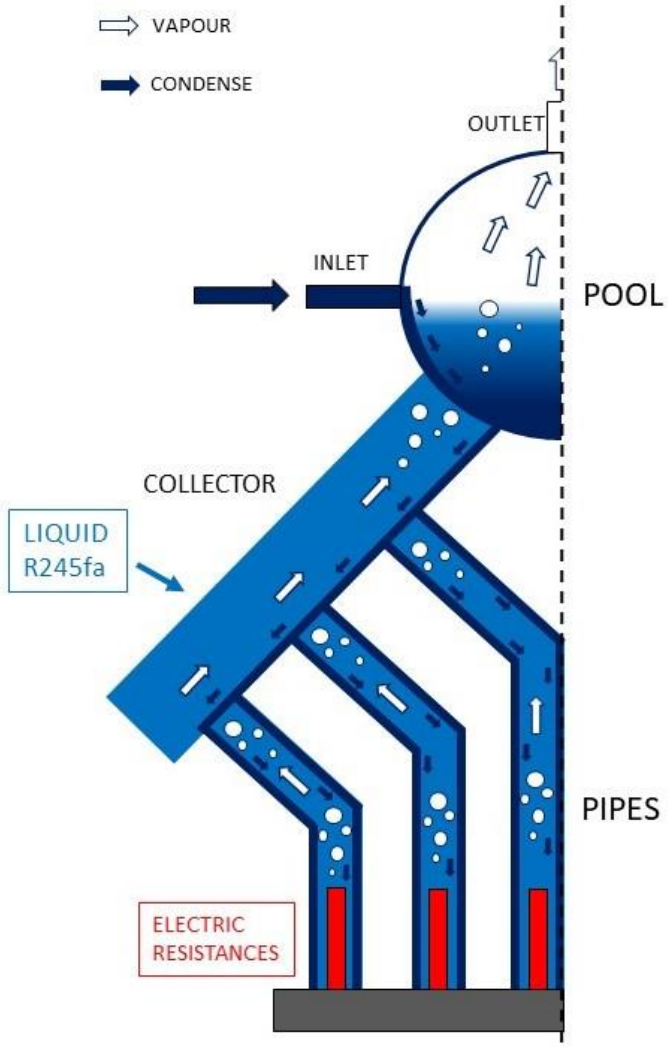

Figure 19. Working principle of the evaporator prototype.

The evaporator working cycle begins with the withdrawn of the saturated liquid coming from the condenser. This liquid, being in this phase colder and therefore denser than the rest of the fluid inside the device, flows adjacent to the walls towards the bottom. Then, when the cold fluid reaches the electric resistances it vaporizes returning to the top and, eventually, is discharged from the evaporator.

3.2.4 Expansion valve

As previously explained, actual energy production is not a priority for this study. Therefore, no machine capable of converting the energy of the fluid into mechanical work has been installed in the system. However, in order to realize a Rankine cycle, fluid expansion is an essential thermodynamic transformation. To meet this need, it was decided to install a manual expansion valve that achieves the desired pressure drop. Nevertheless, the system has been set up to be eventually connected to an expansion machine in the future.

The valve installed is a R120-04CKX54 made of bronze and developed by MECA-FLUID with the following technical characteristics:

Table 4. Expansion valve technical data.

Parameter	Value	U.o.M.
Maximum inlet pressure	30	bar
Adjustment Range	0.5 to 8	bar
Temperature Range	-20 to +130	°C
Flow coefficient Kv	1	m^3/h
Flow rate at maximum pressure	500	l/min

Figure 20. Expansion valve R120-04 MECA-FLUID [22].

3.2.5 Pipelines

All the pipes are in copper and the diameter has been determined to obtain the minimum required speed (0.5m/s for liquid and 10m/s for vapour) at partial load (3 kW):

- 1/2” (12,7 mm) for the liquid
- 1,1/8” (28,575mm) for the vapour

Other important devices have been included in the circuit:

- Filter: A dehydration filter has been placed before the evaporator, to ensure the total absence of water inside the refrigerant fluid and eliminate any particulate circulating in the system.
- Flexible pipes: two flexible pipes have been installed at the inlet and at the outlet of the pump to dampen vibrations and prevent them from spreading in the system.
- Shut-off valves: these valves have been placed between each component in order to allow possible interventions, keeping the rest of the system under pressure.

3.3 Working fluid

ORCs can be designed using a huge number of possible working fluids: this is obviously

a great advantage that makes these systems suitable for almost every heat source but, on the other hand, makes the resolution of the optimization problem inevitably more difficult. Organic fluids can be selected from various chemical classes like hydrocarbons (alkanes, alkenes, etc.), refrigerant fluids (partially fluorinated and perfluorinated compounds), and siloxanes [23].

Only a small number of pure fluids are however commonly used in commercial systems (mainly toluene, pentane, butane, R134a, R245fa, and light siloxanes), because ORC manufacturers tend to keep the choice among a limited number of well-known fluids already used in previous installations [23].

The fluid selected for the present experimental investigation is refrigerant fluid R245fa, which has favourable properties for low temperature heat recovery systems [24], has a low toxicity and is non-flammable.

Table (5) summarizes the physical properties of R245fa while in figure (21) is shown the Pressure-Enthalpy diagram with an example of Organic Rankine Cycle.

Table 5. R245fa physical properties

Boiling point at 1,01 bar	15,3 °C
Freezing point at 1,01 bar	-107 °C
Liquid heat capacity	1,36 $^{kJ}/_{kgK}$
Critical Temperature (°C)	154.01
Critical Pressure (bar)	36.51
Liquid Density (kg/m³) 0°C	1338.54
ANSIASHRAE Standard 36-1992 Safety Group Classification	B1
GWP	1030

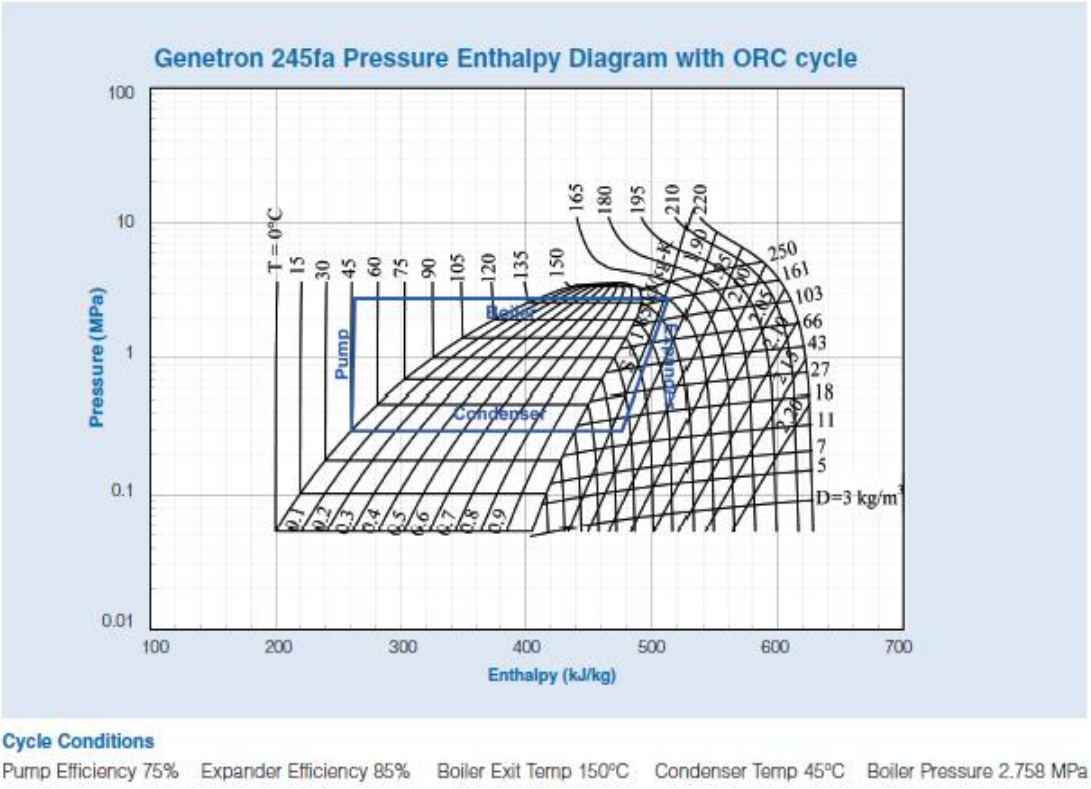

Figure 21. R245fa Pressure-Enthalpy diagram with an ORC cycle [24]

3.4 Measurements and acquisition

This section illustrates the data acquisition system together with the technical specifications of all the sensors used. The measured parameters are: temperature, pressure, differential pressure and mass flow rate. The location of the sensors in the test rig has been shown in figure (15).

3.4.1 Sensors

The variables and sensors used for their acquisition are:

- Temperature: all the temperatures in the system are measured with T-type thermocouples. A thermocouple consists in two wires made from different metals and welded together at one end. When this junction is exposed to a temperature variation, a proportional voltage is created. The voltage can be then converted in a temperature value after an appropriate calibration. With its simplicity, the low cost, a measuring range between -200 °C and +350 °C and an accuracy of $\pm 0{,}5$ K the thermocouple is the most common choice for this kind of application.
- Pressure: absolute pressures and differential pressure are both measured by piezoelectric sensors developed by Keller. A piezoelectric element (metallized quartz or ceramic materials) is a transducer capable of converting stress into an electric potential. All the pressure sensors used present the same output range (4-20 mA) while the input range is summarized in table (6).
-

Table 6. Pressure sensors working range

Sensor	Measured variable	Range [bar]	Accuracy [%FS]
pressure	Pump outlet	0:25	0.5
	Expansion valve inlet	0:25	0.5
	Condenser inlet	0:5	0.5
	Δ Evaporator	0:0.2	0.5

- Mass flow rate: The mass flow rate of the refrigerant R245fa needs to be measured with high accuracy because it strongly affects the calculated performances. This led to choose a Coriolis flowmeter (model OPTIMASS 6400C developed by KROHNE) with an accuracy of 0.1% on the measured value. The graphs, provided by the supplier, showing the accuracy and the pressure drop of the flowmeter as a function of the mass flow rate can be consulted in figure 22.

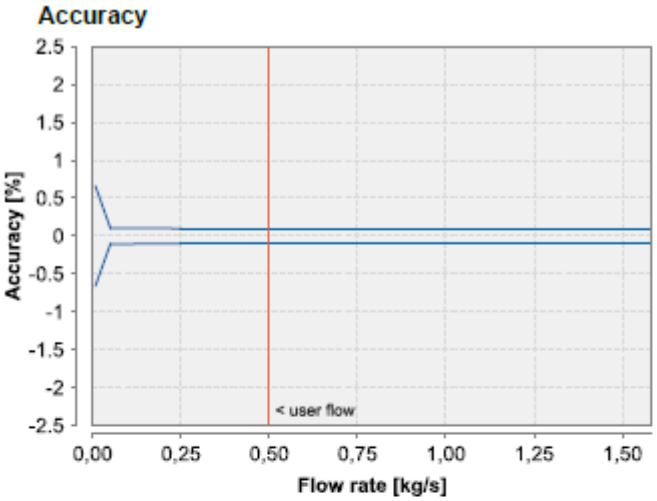

Flow rate [kg/s]	Accuracy [%]
0.0081	0.6552
0.05	0.1056
0.25	0.1
0.3125	0.1
0.375	0.1
0.4375	0.1
0.5	0.1
0.625	0.1
0.75	0.1
0.875	0.1
1.0	0.1
1.583	0.1

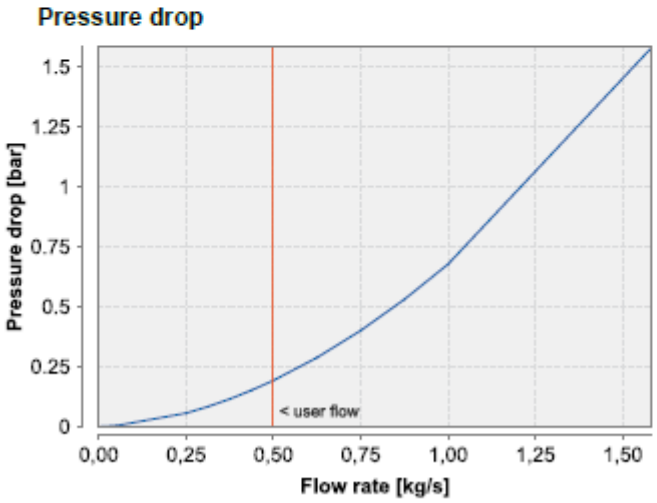

Flow rate [kg/s]	Pressure drop [bar]
0.0081	0.0002
0.05	0.0035
0.25	0.0559
0.3125	0.0831
0.375	0.1149
0.4375	0.1514
0.5	0.1924
0.625	0.2878
0.75	0.4006
0.875	0.5305
1.0	0.6773
1.583	1.581

Figure 22. Diagrams for accuracy and pressure drop of the Coriolis Flow Meter in function of the mass flow rate [25].

- Fluid level: A magnetic level indicator (produced by SPIRAX SARCO, model: "Colima Viscorol") has been installed on the evaporator tank to monitor the amount of liquid inside it. A too low level would, in fact, give rise to the aforementioned Dry-Out phenomenon. Too high a level could lead to complete filling of the evaporator, blocking the circuit. The working range of the installed model is provided by the table (8).

Table 7. Magnetic level indicator technical data

Parameter	Value	U.o.M.
Maximum pressure	125	bar
Temperature range	-25 to +350	°C

3.4.2 Acquisition

The measurement acquisition of all the previous sensors is performed by a CompactRIO (National Instrument, model: cRIO-9067) interacting with a LabView interface which displays the real-time values. The LabView interface also allows the operator to control remotely the test bench.

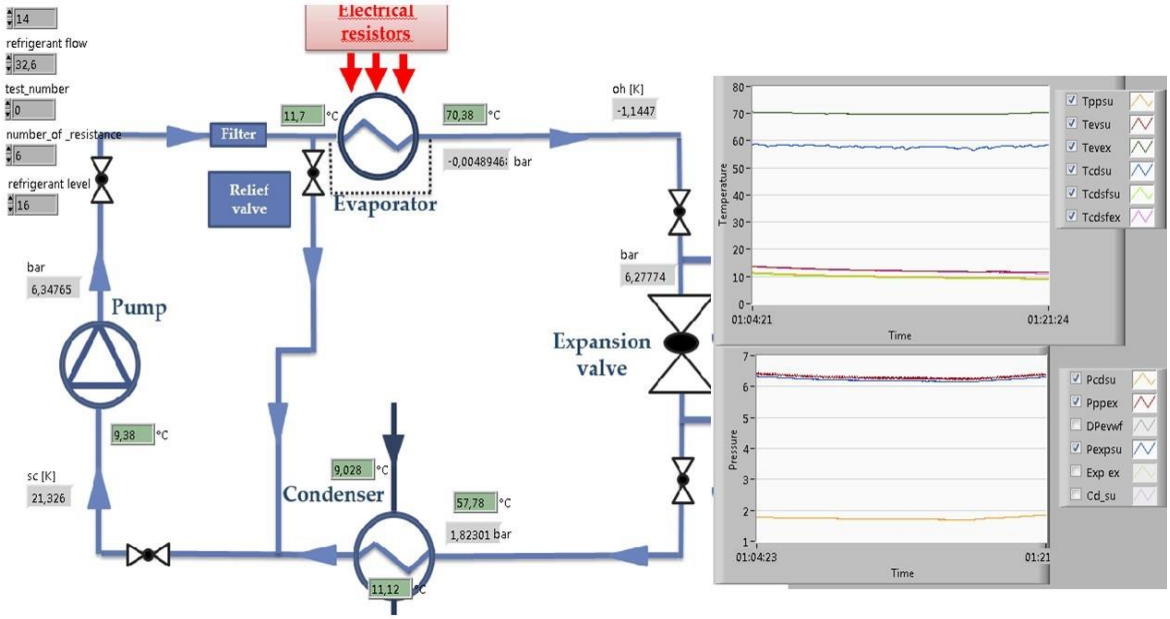

Figure 23. LabView interface for data acquisition.

Data collected after the experimental run (T, P, mass flow, etc.) are post-processed in a steady-state model developed in Matlab to derive the ORC performance.

3.5 Test bench assembly

The assembly phase of the test bench has been realized through the following operations:

- Construction of the load-bearing structure: the structure has been realized using Bosch aluminium profiles with a 45x45 mm cross-section. These profiles guarantee the structure a high rigidity, while maintaining a very low overall weight (the weight of the profiles is only 1.6 kg / m). The junctions between the different profiles have been made using the appropriate brackets, realized by the same supplier. The global structure presents the following dimensions:

    - Height = 1,5 m
    - Width = 1,5 m
    - Depth = 1,2 m

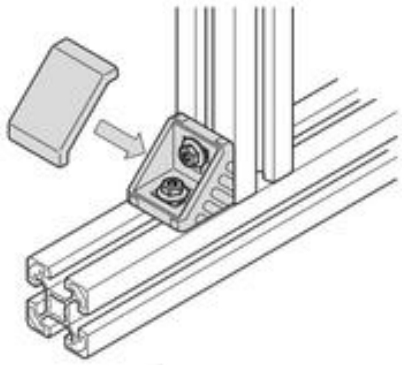

Figure 24. Aluminium profile 45x45 and brackets [26]

- Positioning and fixing of components: Not having particular limits of space, the positioning of the components has been done simply in order to guarantee a uniform weight distribution. The evaporator instead, given its high weight, has been designed with support legs to be able to rest directly on the ground and not on the structure. The fixing of the components has been realized in such a way as to minimize the presence of vibrations (caused by the motor-pump unit). If high, in fact, vibrations could lead to the initiation of cracks in the copper pipes causing leakage of refrigerant

fluid and, not less important, could alter the data acquired by sensors (this is only valid for piezoelectric pressure sensors and the Coriolis mass flow meter).

- Piping construction: Once that the components have been positioned, it has been possible to start the operation of measuring the distances between them, in order to make the copper pipes constituting the circuit. The circuit presents a layout with the least number of elbow bends possible to avoid elevated pressure drops inside of it. In addition to the aforementioned check valves, expansion valve, pressure release valve, dehydration filter and flexible hoses, the installation of the pipes involved also the realization of the measurement sensors housing devices. For the thermocouples, the housing has been made with copper tubes of 4 mm diameter, inserted in the elbows and longitudinally to the flow. The pressure sensors instead, to be connected to the circuit required the installation of small Schrader valves directly in the pipes.

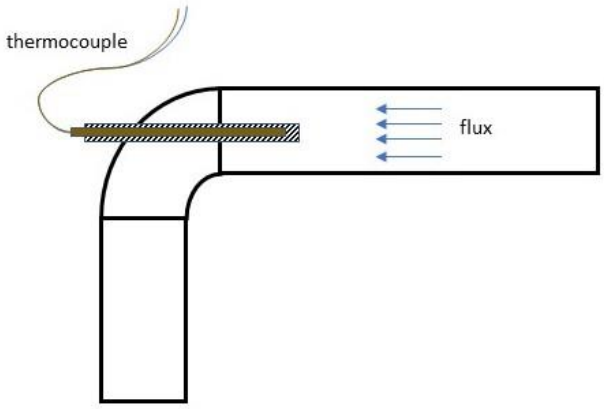

Figure 25. Schematic of the installation of a thermocouple.

- Realization of power circuit and connection of the measurement sensors to the data acquisition device (compactRIO-9067)

3.6 Starting procedure

In this section the starting procedure to prepare the system for carrying out the tests is illustrated.

1. *Start data acquisition*: Some of the operations analysed below are achievable only with a real-time monitoring of temperature and pressure. It is therefore essential to perform the acquisition system as the first operation.
2. *Tightness test*: Because of the high number of welds on the pipes and the several joints realized between the various components, it is impossible to guarantee the total absence of leaks in the system a priori. Since the loss of refrigerant would be primarily harmful to the environment and secondly, it would strongly alter the experimental analysis, it is essential to perform a tightness test before filling the system with the working fluid. To perform the tightness test, a quantity of nitrogen is introduced into the system until the desired pressure value is reached. Since not all pressure sensors have the same working range (see table) the test has been performed on two pressure levels. A first test has been performed at 5 bar and the second one at 20 bar after disconnecting the sensor at the condenser inlet (which endures a maximum pressure of 5 bar). Once the pressure level has been reached, the trend of the latter is monitored as a function of time, thanks to the real-time acquisition of data. A significant pressure drops over a short period of time is a sign of the presence of leaks in the system. After repairing the worst losses, it becomes difficult to assess the presence of minor losses, simply by monitoring the pressure trend in the short term. Furthermore, the pressure in the system is closely linked to the temperature trend in the room, which can vary substantially throughout the day. It is for this reason that to check the total absence of leaks in the system it is necessary to monitor the pressure and temperature trends within 24 hours. In this way it is possible to evaluate whether in two different times when the room is at the same temperature, the pressure values are the same.
3. *Check if all valves are opened (bypass valve included):* During the tightness test, it is frequent that some check valves are closed to isolate some parts of the circuit in order to more easily detect leaks.

4. *Creation of the void*: Before start filling with the working fluid, it is necessary to remove all the air and to create the void inside the system. The operation has been carried out by connecting a vacuum pump to the circuit.
5. *Filling with R245fa*: The amount of refrigerant liquid required by the system has been calculated determining first the volume of the pipes (only the liquid side since vapour presents a neglectable density), the inner volume of the condenser and the inner volume of the evaporator (the latter is filled until a level of liquid equal to 1/3 of the tank is reached). The overall volume has been then multiplied by the density of the refrigerant ($\rho = 1350\ \frac{kg}{m^3}$ at 5 bar and 20 ° C) to obtain the required mass of liquid (which is 34 kg).
6. *Supply the condenser with water*: Supplying the condenser with water reduces the temperature of the components and of the refrigerant, decreasing consequently the pressure inside the circuit and facilitating the filling phase.
7. *Start the electrical load*: The electric resistances are switched on and the temperature and pressure inside the evaporator gradually increase.
8. *Start the working fluid pump:* As the temperature and pressure increase, the pump must be started in order to allow the vapour to condense.
9. *Adjust pump rotational speed and expansion valve to the desired value*

3.7 Anomalies found

During the first ignitions of the electrical resistance group, an anomaly occurred, and the differential switch interrupted the current flow. The problem was caused by an error in the evaporator design. The housing for the resistances inside the evaporator tubes, in fact, had a diameter of 8 mm higher than the diameter of the resistors, thus preventing a direct metal-metal contact. The air trapped between the wall of the electrical resistance and the wall of the steel pipe constitutes a highly insulating layer which, during the first ignition has caused an excessive overheating of the resistances and their damage.

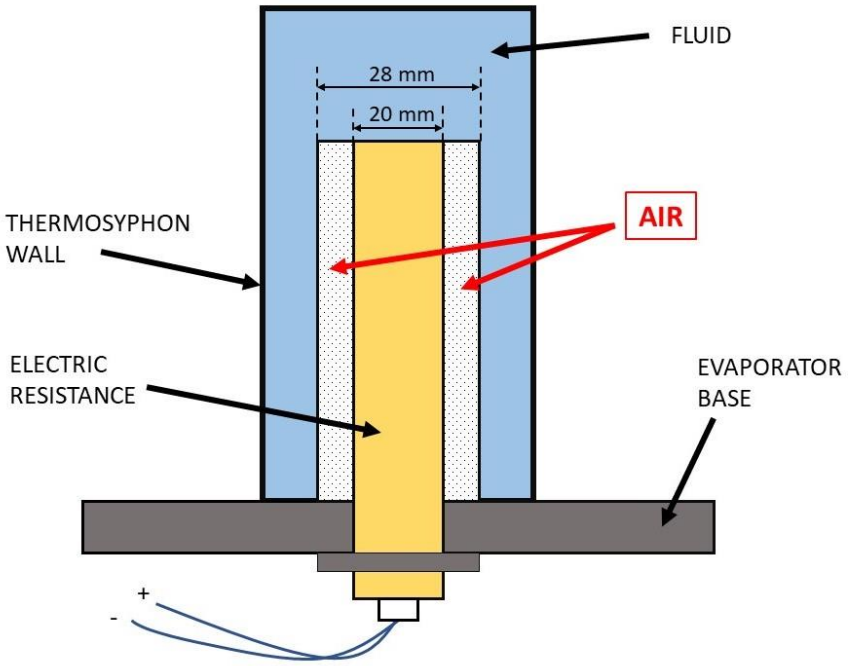

Figure 26. Schematic of the anomaly found on the electric resistances.

Various solutions for solving the problem have been taken into consideration:

1. Intervene on the evaporator geometry: One of the most effective solutions would have been to remove the evaporator and work on it first by enlarging the holes in the base, through which the resistances are inserted, in order then to insert a steel tube of the exact dimensions of the cavity. The solution is illustrated in figure:

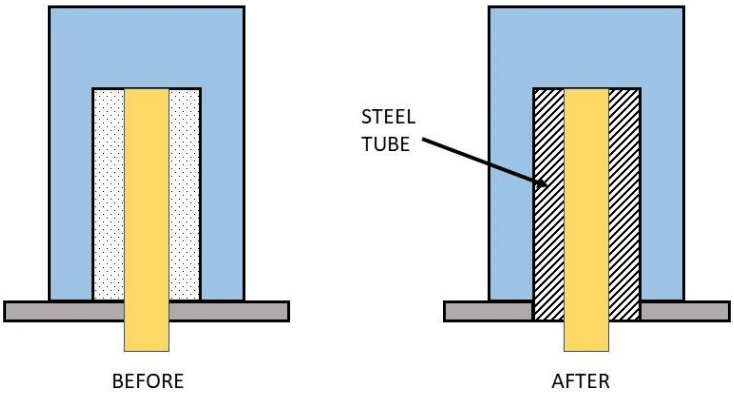

Figure 27. Schematic of the "Tube solution" for the electric resistances.

The realization of this intervention would have required the extraction of all the refrigerant fluid from the system (a process considerably longer than the filling operation), the desoldering of the copper pipes at the inlet and outlet of the evaporator and their subsequent welding after the intervention. Moreover, also the enlargement of the holes on the evaporator would have been complex due to the size and the particular geometry of the latter. Therefore, it has been decided to opt for a solution that did not require removal of the evaporator from the test bench.

2. Filling with oil: In order to fill the volume of air and create a layer capable of easily conducting heat, the idea of realizing a system that constantly pumps oil into the housing has been evaluated. Although the solution is certainly valid from the performance point of view, its realization would have been too complex, causing delays in the execution of the tests.

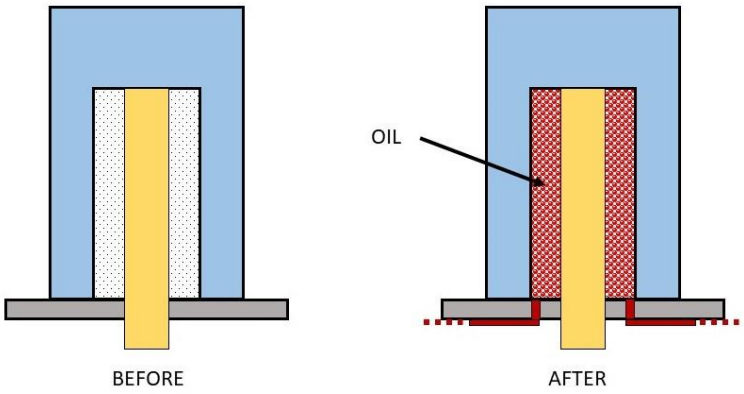

Figure 28. Schematic of the "Oil solution" for the electric resistances.

3. Installation of steel shims: The solution that finally has been chosen, consists of making shims to be inserted between the electric resistance and the evaporator wall in order to favour heat conduction. The shims have been made by longitudinally dividing some appropriate-size steel pipes, into 4 parts. The solution is illustrated in figure:

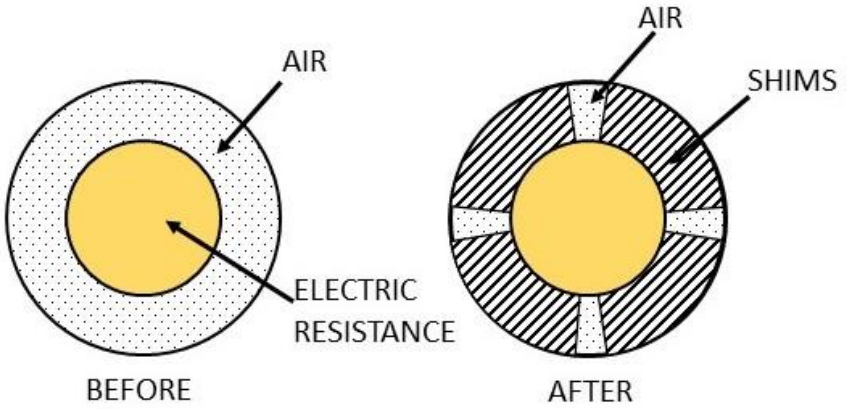

Figure 29. Schematic of the "Shims solution" for the electric resistances.

The solution just exposed, although not optimal because it does not eliminate the whole volume of air, has been chosen because it is able to bring significant benefits with a relatively simple realization. However, both because the construction and installation of these components has delayed the execution of the tests, and because it was impossible to forecast the stability of this solution in the long run (remember that a small volume of air is still present in the housing of the resistances) it was decided to carry out an experimental campaign limiting the thermal power to half of the maximum exploitable one, that is using only 8 electric resistances that provide a total power of 12 kW.

3.8 Experimental Results

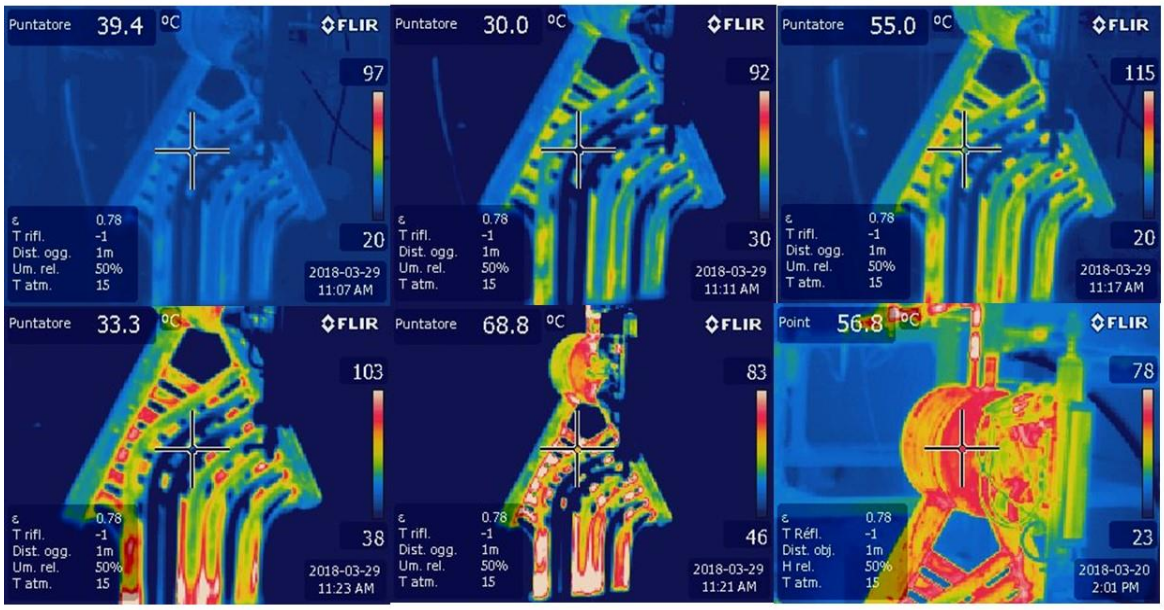

Figure 30. Sequence of photos, acquired with a thermal camera, of the thermodynamic evolution of the evaporator.

The experimental campaign has been carried out to characterize the system performance under various steady-state operating conditions within the working range imposed by the various components.

Globally, 27 steady-state points have been collected by opportunely varying the electric power, the mass flow rate by means of the inverter and the pressure at the outlet of the evaporator by acting on the expansion valve.

3.8.1 Assessing the quality of the data

The procedure for reaching the stationary conditions, and the subsequent recording of the data, consists in acting on the previously mentioned parameters (electric power, mass flow rate and pressure at the evaporator outlet) until the desired working conditions are reached. First, the thermal power is set by selecting the number of active electric resistors, then the pressure is imposed on the evaporator outlet by acting on the expansion valve and finally the system is stabilized by adjusting the mass flow rate appropriately. After the system

stabilization has been achieved, by monitoring the trend of the variables through the LabView interface, the data acquired by the sensors are recorded over a set time interval of 5 minutes. At this point, the post-processing phase of the data, through a code elaborated on MATLAB, starts. The aim is to obtain work points that can be considered acquired in steady-state conditions, averaging the values previously recorded over the 5-minute period.

Because the measured numerical values are subject to different uncertainties, possible errors or sensor malfunction, a second process is necessary to assess the quality of the data. The method that has been used is to verify energy balances in each component for every steady-state point.

Evaporator

The evaporator is subject to heat exchanges with the environment. For this reason, the application of the first law of thermodynamics is not only useful for verifying the quality of the data obtained from the sensors but also provides an initial assessment of the extent of such losses with the environment. The energy balance applied to the exchanger results as follows:

$$\dot{Q}_{el} - \dot{Q}_{ev,lost} = \dot{m} \cdot \left(h_{ev,ex} - h_{ev,su}\right) \tag{40}$$

Where

$\dot{m} \cdot \left(h_{ev,ex} - h_{ev,su}\right)$ is the thermal power exchanged by the fluid in the evaporator which from now on will be called: $\dot{Q}_{ev}$

$\dot{m}$ is the mass flow rate of the refrigerant $\left[\frac{kg}{s}\right]$.

$h_{ev,ex}$ and $h_{ev,su}$ are the enthalpy of the fluid at the outlet and inlet of the evaporator, respectively, $\left[\frac{J}{kg}\right]$

$\dot{Q}_{ev,lost}$ is the thermal power transferred to the environment, [W]

The electric power has been calculated simply by multiplying the power of a single resistor by the number of active resistors.

$$\dot{Q}_{el} = n \cdot \dot{Q}_R \tag{41}$$

Where

$\dot{Q}_R = 1500$ [W], is the electric power of each resistance installed.

The graph obtained from comparing the electric power and the thermal power exchanged in the evaporator is the following:

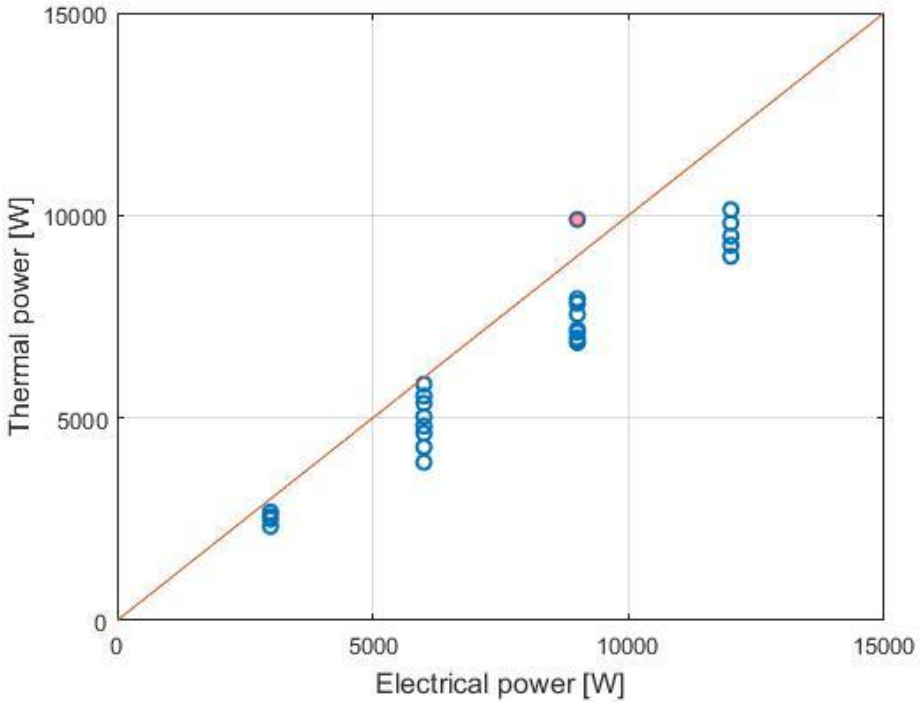

Figure 31. Graph comparing the electric power with the thermal power in the evaporator

Except for one point (marked in red), which is a non-physical point resulting from an error as the thermal power exchanged in the evaporator cannot exceed the electric power, the graph shows a coherent trend. In fact, as the electrical power grows, the difference between it and the thermal power increases as well. This is due to increasing heat losses with the environment when high temperatures are reached.

Overall, the results obtained after this initial analysis have proved to be promising and have not highlighted any particular anomalies in the acquisition of data.

Expansion valve

The control phase proceeds by examining the energy balance across the expansion valve. The expansion valve, under ideal conditions, is an organ capable of providing a pressure drop maintaining the same enthalpy level between inlet and outlet. Considering the thermal exchanges with the environment, the formulation of the first principle of thermodynamics is as follows:

$$\dot{Q}_{v,loss} = \dot{m} \cdot \left(h_{v,ex} - h_{v,su}\right) \tag{42}$$

Where

$\dot{Q}_{v,loss}$ is the thermal power exchanged with the environment [W]

$h_{v,ex}\ and\ h_{v,su}$ are the enthalpy of the fluid at the outlet and inlet of the valve, respectively, $\left[\frac{J}{kg}\right]$

The graph obtained by comparing the enthalpy level at the inlet and outlet of the expansion valve is the following:

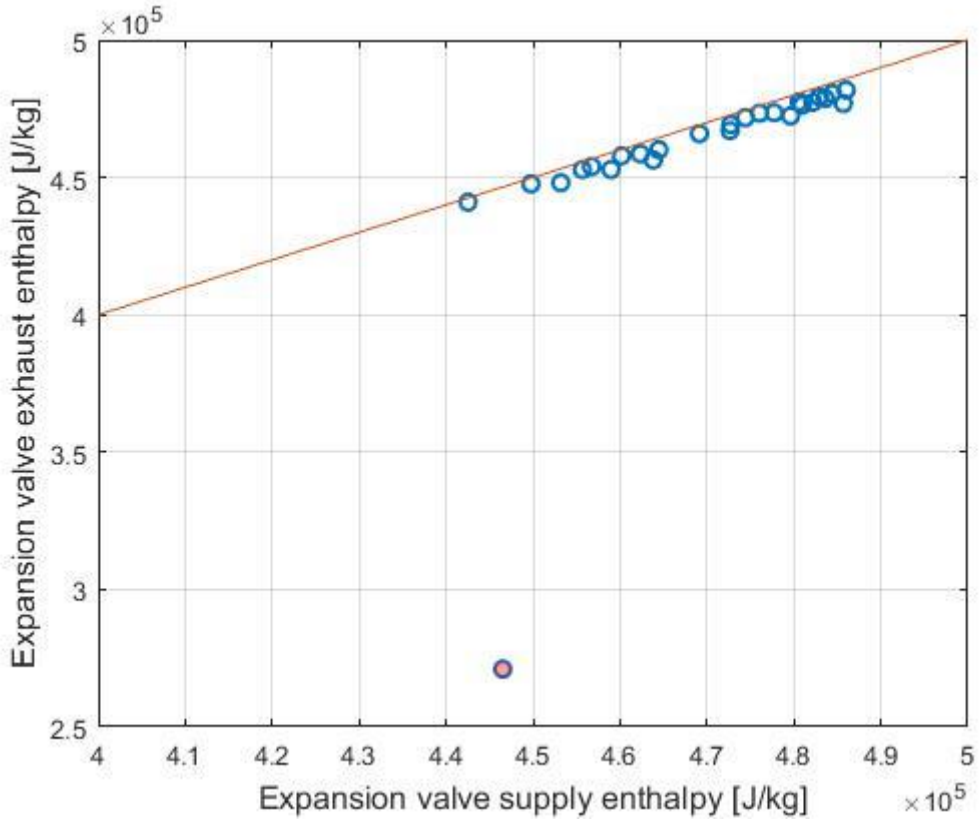

Figure 32. Enthalpy level before and after the expansion valve

Even in this case, there is only one point (marked in red) that shows an important deviation from the rest of the results. This is probably due to an error of the author or a malfunction during the execution of the test. The rest of the graph shows excellent results highlighting minimum energy losses. The result is in line with expectations as the expansion valve is a relatively small component and consequently, the heat exchange surface is limited.

ORC system

In the end, it has been decided to check the energy balance of the entire cycle:

$$\dot{Q}_{ev} - \dot{Q}_{cd} + \dot{W}_{pp} = 0 \tag{43}$$

Where

$\dot{Q}_{ev}$ is the thermal power provided by the evaporator, [W], calculated as in (40)

$\dot{Q}_{cd}$ is the thermal power absorbed by the condenser, [W], given by:

$$\dot{Q}_{cd} = \dot{m} \cdot \left(h_{cd,ex} - h_{cd,su}\right) \tag{44}$$

$h_{cd,ex}\ and\ h_{cd,su}$ are the enthalpy of the fluid at the outlet and inlet of the condenser, respectively, $\left[\frac{J}{kg}\right]$

$\dot{W}_{pp}$ is the mechanical power transferred to the fluid from the pump [W], given by:

$$\dot{W}_{pp} = \frac{\dot{m} \cdot \left(p_{pp,ex} - p_{pp,su}\right)}{\rho} \tag{45}$$

Where

$p_{pp,ex}\ and\ p_{pp,su}$ are the pressure of the liquid at the outlet and inlet of the pump, respectively, [Pa]

ρ is the density of the refrigerant liquid $\left[\frac{kg}{m^3}\right]$

The graph used to check whether the power input and output of the system coincide at the global level is as follows:

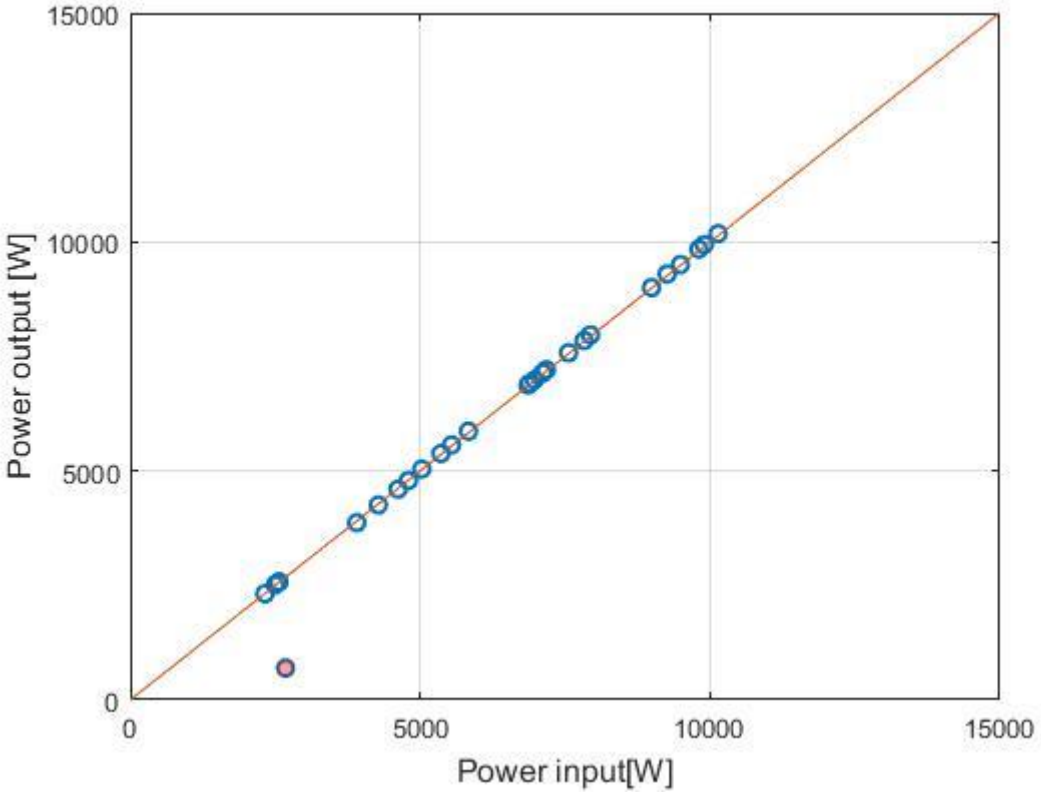

Figure 33. Evaluation of the ORC energy balance.

Except for the same anomalous point already highlighted above, the graph shows a perfect correspondence between the input and the output power values of the system. This result provides further confirmation regarding the quality of the acquired data.

To conclude, the control just carried out through thermal balances has shown excellent results for almost all the data acquired. This means that there are no measurement errors that could affect the interpretation of the results and that it is therefore possible to continue with the experimental analysis.

3.8.2 Range of operating conditions

The choice of the working conditions of the system during this experimental investigation has been made taking into account a series of operating limits imposed by the installed components. The operating limits that most influenced the experimental campaign have been the following:

- Maximum electric power: 12 kW (reducible to 3, 6 and 9 kW)

- Maximum pressure at the outlet of the evaporator: 25 bar (imposed by the absolute pressure sensor, see table)

- Maximum pressure at the outlet of the expansion valve: 6 bar (imposed by the gauge pressure sensor, see table)

- Maximum temperature: 130 °C (imposed by the expansion valve, see table)

- Minimum and maximum level of liquid inside the evaporator:

An additional limit is represented by the level of liquid inside the evaporator (measured by the magnetic indicator). It was, in fact, necessary to verify for each working condition of the system that the liquid level was not too low (risk of the dry-out phenomenon) or too high, to the point of completely filling the evaporator and blocking the system. The magnetic level indicator returns a value between 0, which corresponds to a volume of liquid inside the evaporator of 0.0223 m^3 and 20, to which corresponds a volume of liquid equal to 0.0323 m^3 which for safety reasons has been taken as the maximum level reachable.

In light of these considerations, the variation of the parameters explored during the whole experimental analysis is summarized in table (8)

Table 8. Range of achieved operation conditions

Working Condition	Minimum value	Maximum value
Electric power	3000 W	12000 W
Evaporator thermal power	2323 W	10140 W
Evaporator pressure	3,51 bar	20,04 bar
Condenser pressure	1,05 bar	5,97 bar
Evaporator exhaust temperature	49,8 °C	121,3 °C
Condenser supply temperature	43,55 °C	93,06 °C
Mass flow rate	0,0095 kg/s	0,0390 kg/s
Volume of liquid inside the evaporator	0,0268 m^3	0,0308 m^3

An indicative graph showing the working areas explored during the tests performed is as follows:

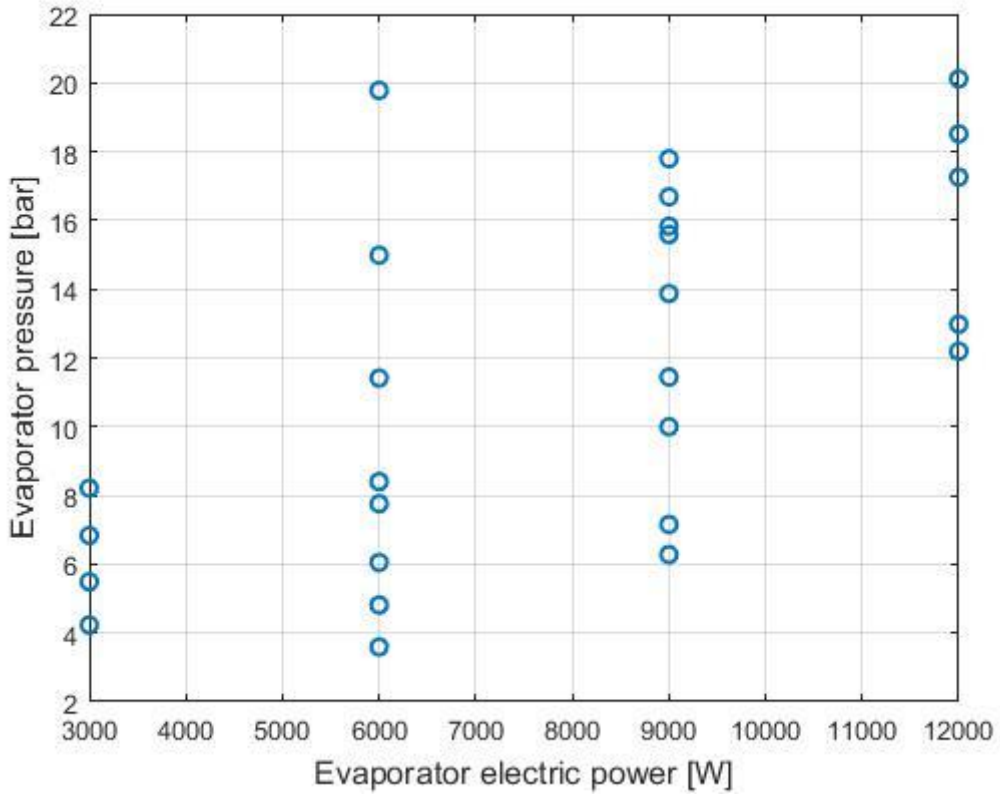

Figure 34. Evaporator pressure in function of the electric power.

The graph shows the variation of the pressure level reached in the evaporator in function of the electric power used for every steady-state point that has been analysed. The most evident fact is that for low powers (3 kW) it has not been possible to reach high pressures inside the evaporator, while vice versa when using the maximum power (12kW), the minimum pressure reached has been about 12 bar. The system has instead shown a wide operating range when using intermediate powers (6 and 9 kW), especially with 6 kW, allowing an adjustment that varies from a few bars, until reaching the maximum pressure value of the whole experimental analysis (20 bar).

3.8.3 Performance

The study of the performances is limited to the evaporator (component of which this thesis is concerned) and the thermodynamic cycle. For the latter, the thermodynamic

transformations are shown on a Temperature-Entropy diagram and some of the most important aspects for an organic Rankine cycle, i.e. sub cooling, overheating and pitch point, are discussed. For the evaporator, on the other hand, the analysis focuses on the losses of thermal power and pressure to which this component is subjected, as well as on the variation in volume of liquid that occurs inside it.

Evaporator performance

The first parameter that has been taken into consideration for the evaluation of the evaporator performance is the loss of heat that has occurred in the environment. The results are shown in the following graph:

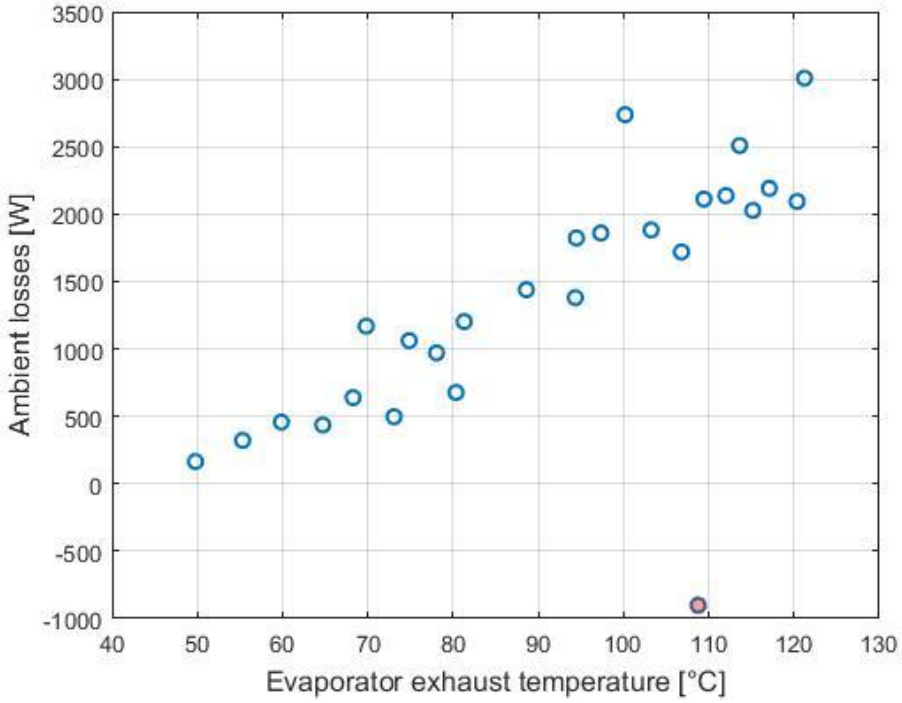

Figure 35. Ambient losses in function of the evaporator exhaust temperature.

Where the thermal power lost in the environment has been calculated by equation (40).

The graph shows the thermal power transferred to the environment in function of the temperature at the outlet of the evaporator. The magnitude of the lost power obviously grows with the increase of the temperature reached in the evaporator, due to the great difference in

temperature that is established between the latter and the room. It is also evident that the power exchanged with the outside reaches decidedly high values at high temperatures, thus affecting the performance of the evaporator. In fact, these losses reach values between 2000 and 3000 W in the temperature range of 100-120 ° C.

To better understand the impact of these losses it may be useful to analyse the graph in Figure (35) which shows the thermal power transferred to the environment in relation to the electric power exploited by the evaporator.

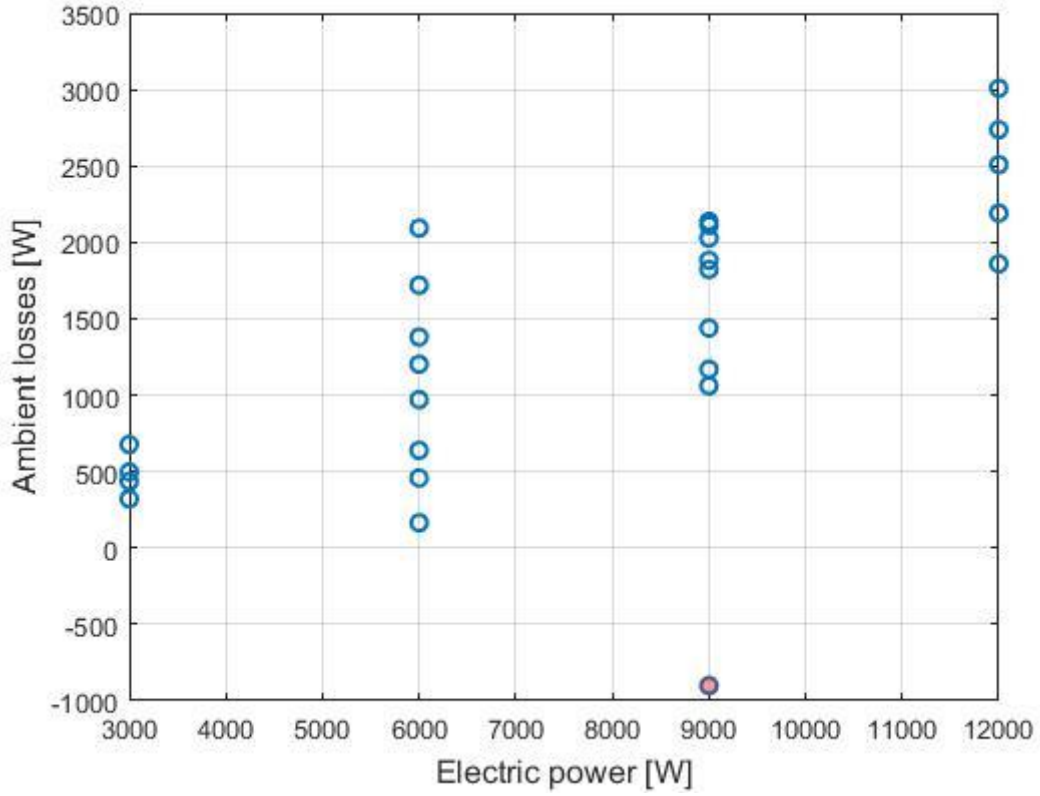

Figure 36. Ambient losses in function of the electric power.

Also in this case, it is evident that the greatest losses of thermal power occur at the maximum electrical power (12000 W). However, the greatest impact occurs at the intermediate power of 6000 W. In this case, in fact, the power exchanged with the environment exceeds 2000 W in one of the test performed at high temperature, resulting equal to 1/3 of the installed electrical power.

This result highlighted a serious problem of thermal insulation of the evaporator with respect to the surrounding environment. It is evident that better results can be achieved by repeating the tests after the installation of an appropriate insulation.

The second parameter that is interesting to analyse in order to evaluate the evaporator performance is the presence of pressure drops introduced by it. The objective has been reached by analysing the following graph:

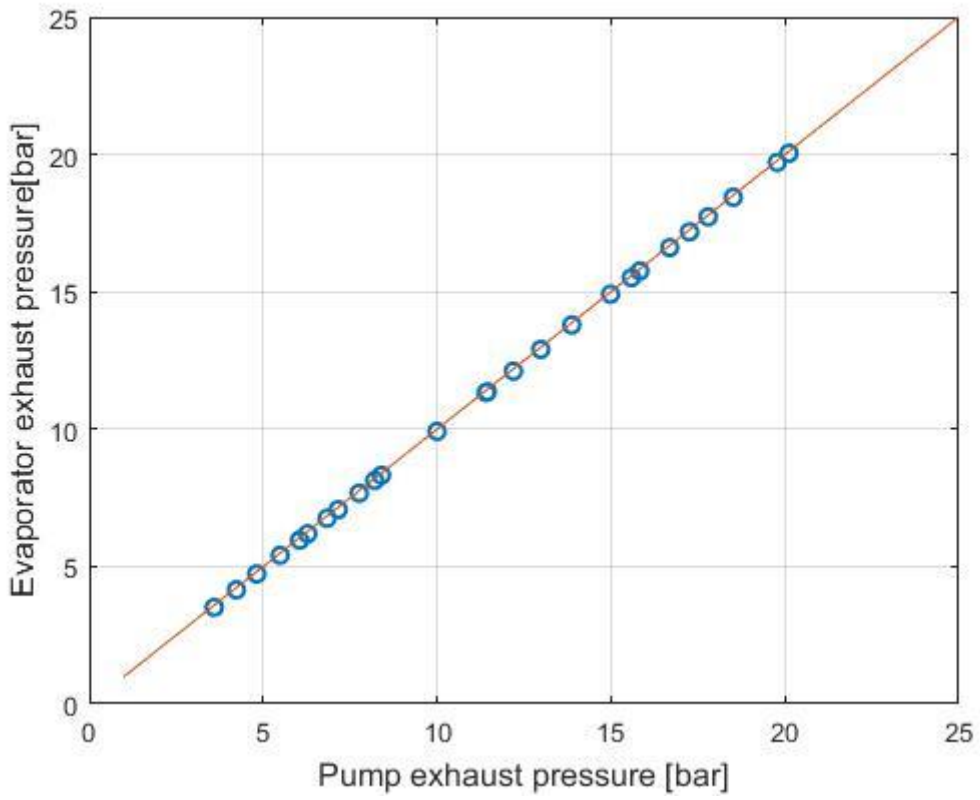

Figure 37. Evaluation of the pressure drops between the pump and the evaporator outlet.

The graph compares the pressure values at the pump outlet with the pressure values at the evaporator outlet. The results obtained are excellent and show almost zero pressure losses both as regards the evaporator and for the whole section of piping that connects the pump with it. This condition is optimal for the pump. In the event of high-pressure losses, in fact, the pump would be forced to perform more work to guarantee a given pressure at the evaporator outlet, with a consequent greater consumption and shortening of its life.

From the point of view of pressure losses, therefore, no anomaly has been found and no further improvement can be realized in the system.

Finally, a parameter that needs to be analysed and discussed to characterize the evaporator behaviour is represented by the level of refrigerant liquid reached inside of it during the various working conditions of the system. To perform this analysis, it is possible to use 3 different graphs showing the variation of the fluid level as a function of: mass flow rate, evaporator temperature and value of sub-cooling reached by the liquid at the condenser outlet.

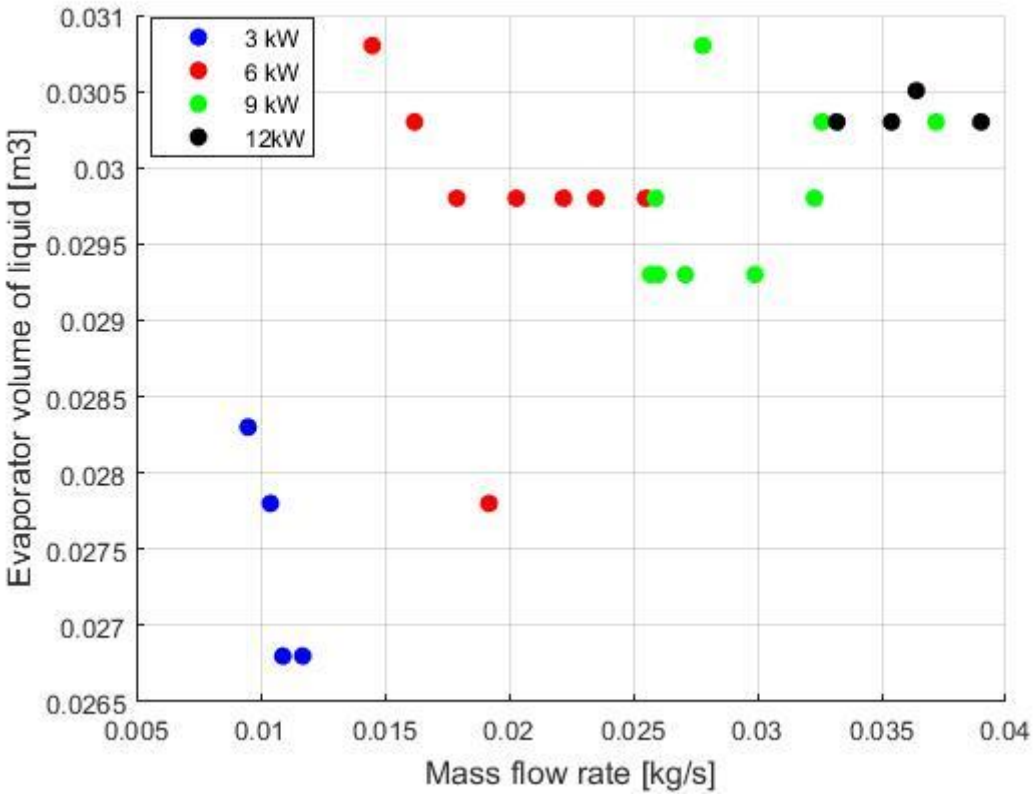

Figure 38. Liquid level inside the evaporator in function of the mass flow rate.

First, the graph related to mass flow is discussed. The results generally show an increasing trend of the volume of liquid as the mass flow rate increases. Although high levels of liquid can also occur at intermediate mass flow rates, thus demonstrating a dependence on other factors, it is evident that the more refrigerant flow increases, the more the evaporator tends to fill. It has proved impossible to work at high mass flow rates while maintaining a low level of liquid in the evaporator. Considering that the maximum power used in this

experimental campaign (12 kW) is half of the maximum power with respect to which the system has been sized (24 kW), these results raise some concerns. In fact, it is recalled that the maximum volume that can be reached in the evaporator is 0.032 m^3. As can be seen from the graph, this value has been almost reached during this series of tests, leaving to assume that it can be exceeded if power and mass flow rate are further increased.

A trend similar to that of the previous case is also shown in the graph that relates the volume of liquid to the temperature reached in the evaporator.

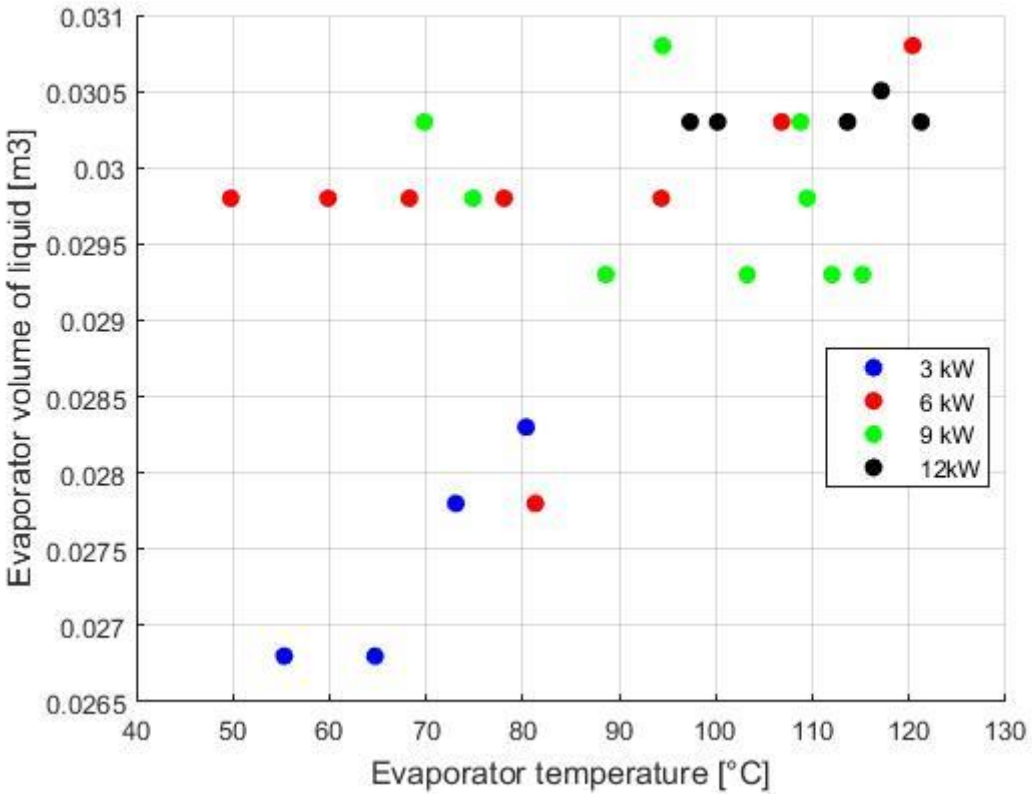

Figure 39. Liquid level inside the evaporator in function of the evaporator temperature.

It also emerged from this analysis that, although in some cases the level of liquid proved to be high even for relatively low temperatures, the peaks were reached at the highest temperatures. This could be related to the volume dilation of the liquid. In fact, with high temperatures, a volumetric expansion of the liquid inside the evaporator is inevitable and this may have partly influenced the increase in the overall level.

It is becoming clear that the behaviour of the fluid level inside the evaporator cannot be characterized by a single parameter but is the result of the combination of several factors. For this reason, the analysis continues by evaluating another parameter that could influence the variation of the amount of liquid inside the evaporator, i.e. the value of sub-cooling at the outlet of the condenser (Figure 39).

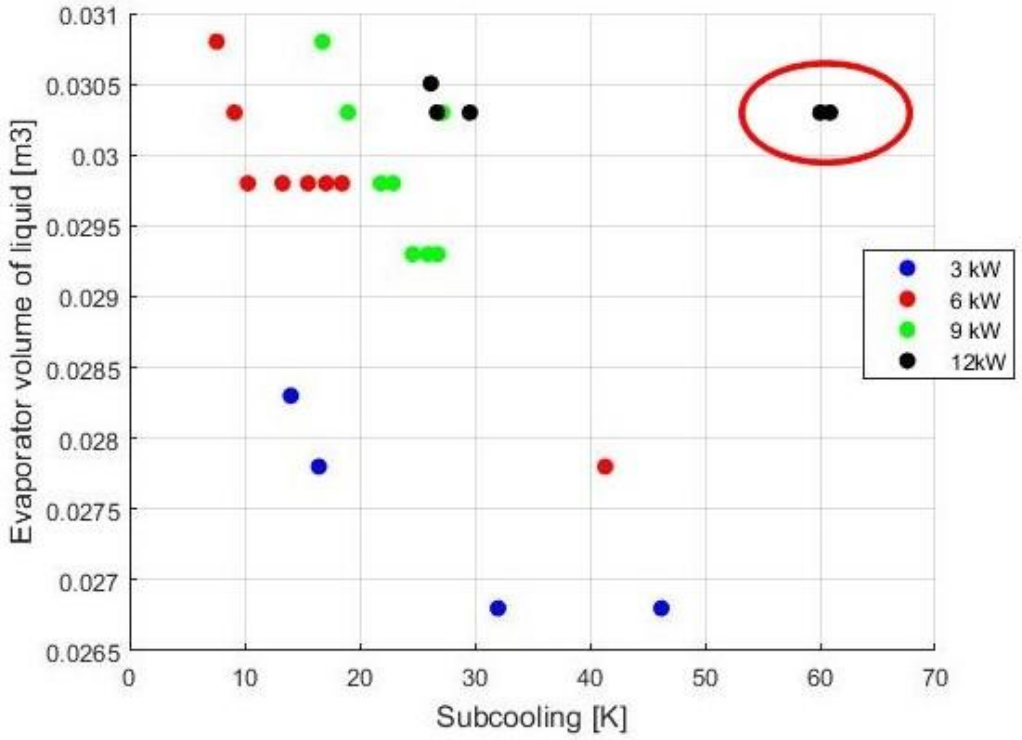

Figure 40. Liquid level inside the evaporator in function of the sub cooling value.

This graph is probably the most significant, showing a regular decrease in the volume of liquid inside the evaporator as the sub-cooling value increases. The sub-cooling value has been obtained as the difference between the saturation temperature of the refrigerant (at the condenser pressure) and its temperature at the condenser outlet:

$$\Delta T_{sc} = T_{cd,sat} - T_{cd,ex} \tag{46}$$

The decreasing trend shown in the graph is explained by the fact that high sub cooling (other conditions being equal) occurs when there is a considerable amount of liquid mass inside the condenser. Being a closed circuit, the mass of liquid tends to be distributed between the condenser and the evaporator since these are the components with the highest volume. It is therefore evident that the more liquid is present in the condenser, the lower the level in the evaporator is and vice versa. From these considerations, the two points circled in red in figure (39) are to be excluded, since their measurement (as shown in the graph in figure 40) took place working at high condenser inlet pressures. In fact, the saturation temperature grows with increasing pressure. This results in a high sub cooling for these points, regardless of the mass of liquid inside the condenser.

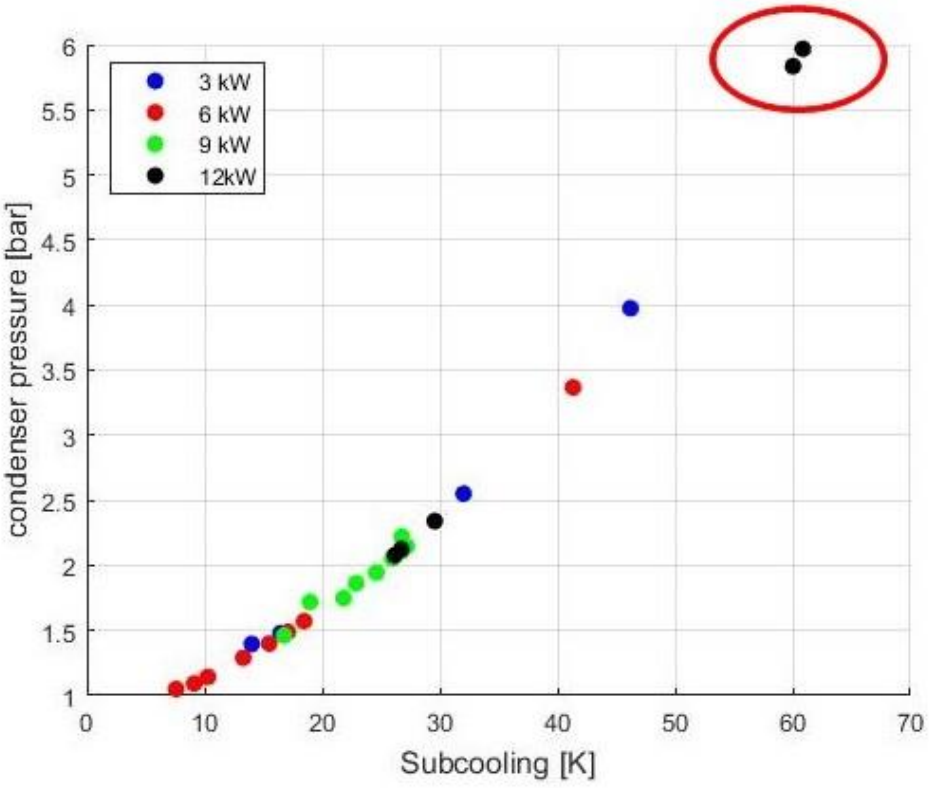

Figure 41. Condenser pressure in function of the sub cooling value.

The volume of liquid inside the evaporator has proved to be a crucial aspect, greatly influencing the experimental campaign carried out since it has almost reached the maximum level in different working conditions of the system. However, it emerged from the analysis of the graphs that this parameter turns out to be in a complex equilibrium dependent on several factors, such as the mass flow rate, the temperature in the evaporator and the saturation temperature of the fluid in the condenser. A model could certainly help to better understand the behaviour of the evaporator and then evaluate on which parameters to intervene to reduce excessive filling in certain working conditions.

Conclusions

Despite the experimental campaign being limited by the maximum usable thermal power, it highlighted important aspects concerning evaporator performance. First, the great thermal power exchanged with the outside through the walls, demonstrating the need to provide appropriate insulation on the external surface of the evaporator. The analysis of pressure drops has instead given excellent results, showing an almost ideal condition. Finally, the study of the variation of the volume of liquid inside the evaporator has raised some concerns in anticipation of the tests that will be carried out in the future increasing the power. A conclusion that can be made in this regard is that it will probably be necessary to adopt solutions to keep the level of liquid under control and to avoid it to reach too high values. One possible solution is to install a liquid receiver downstream of the condenser. A liquid receiver consists of a manually adjustable tank, capable of storing a certain amount of liquid thus avoiding a high evaporator charge. Installations of this type are typical of ORCs in which the heat source does not maintain a constant temperature over time, thus causing imbalances in the load of heat exchangers. In the opposite case of ORCs in which the temperature of the heat source remains almost constant, it is possible to introduce the right amount of refrigerant into the system without the need for a receiver that regulates the level reached in the exchangers. In the case examined in this study, if at the high powers even a receiver of liquid is not sufficient to regulate the level in the evaporator, it would be necessary to review the sizing of the same, providing an increase in its internal volume.

ORC performance

The analysis regarding the performance of the cycle will be performed in this section using a single steady-state point as a reference. The steady-state point that has been chosen presents the following operative conditions:

Table 9. Operating parameters of the reference point.

Electric Power	Mass flow rate	Condenser inlet pressure	Evaporator outlet pressure	Condenser inlet temperature	Evaporator outlet temperature
6 kW	14,5 g/s	1,05 bar	19,71 bar	80,32 °C	120,36 °C

The aspects discussed, and the considerations made, are valid also for all the other points acquired in this experimental campaign.

The ORC is represented on the following Temperature-Entropy diagram:

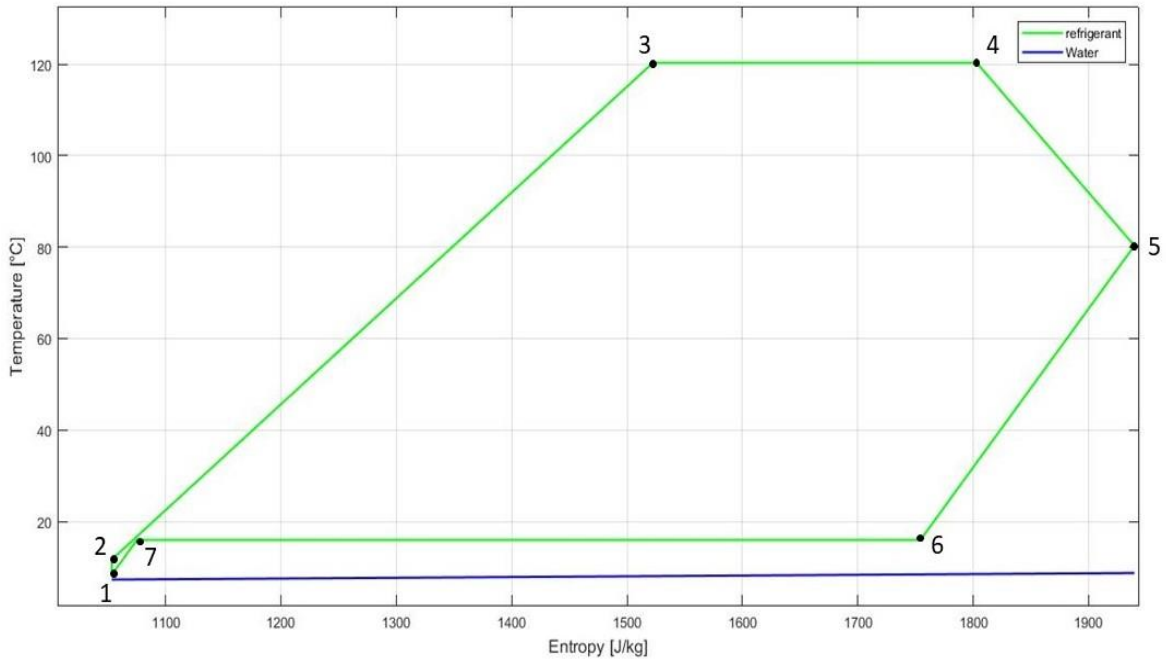

Figure 42. ORC represented on a T-s diagram.

The thermodynamic transformations realized by the cycle are:

- 1-2: Corresponds to the compression made by the pump. The result obtained confirms what has been announced in section 1.4.1, i.e. that the work performed by the pump for the compression is very small and can be neglected.

- 2-3: The liquid phase enters the evaporator, increasing its energy and reaching the saturation temperature in point 3.
- 3-4: During this thermodynamic transformation, carried out at constant temperature (that is the saturation temperature), the evaporation of the liquid phase takes place inside the evaporator.
- 4-5: The vapour at high-enthalpy level exiting the evaporator performs a quasi-iso-enthalpic expansion through the expansion valve, reducing its temperature and pressure. The expansion phase, in a typical ORC, is carried out by a turbine or a volumetric expander, providing a mechanical power as an output
- 5-6: In this phase, the vapour coming out of the valve enters the condenser and is cooled until the saturation temperature is reached.
- 6-7: The vapour during this transformation condenses at a constant temperature.
- 7-1: Finally, the condensed liquid undergoes further subcooling inside the condenser and returns to the pump inlet in conditions 1, completing the cycle.

The most evident feature of the cycle is represented by the presence of the expansion valve which causes a large variation of entropy during the transformation from 4 to 5. In place of the valve, a turbine or a volumetric expander would achieve a high enthalpy jump with a consequent reduction of the final entropy reached and an output fluid closer to the saturation conditions. An excellent result has been obtained from the sub-cooling, which in this case is equal to 8 ° C. This aspect is very important for the working conditions of the pump: ensuring a certain level of sub-cooling at the outlet of the condenser eliminates the risk for the pump to work with a two-phase fluid and therefore in the presence of cavitation. Closely connected to the sub-cooling there is another factor that provides information on the behaviour of the analysed cycle and especially of the condenser, i.e. the pinch-point. The pinch point, which from now on will be indicated with ΔT_{pp}, is defined as the minimum difference between the temperature of the refrigerant and the water inside the condenser. As shown by the magnification of the thermodynamic cycle shown in figure (), the ΔT_{pp} is slightly larger than 1 ° C. This result highlights a great efficiency of the condenser, which manages to bring the refrigerant liquid almost to the same temperature as the inlet of the cooling water.

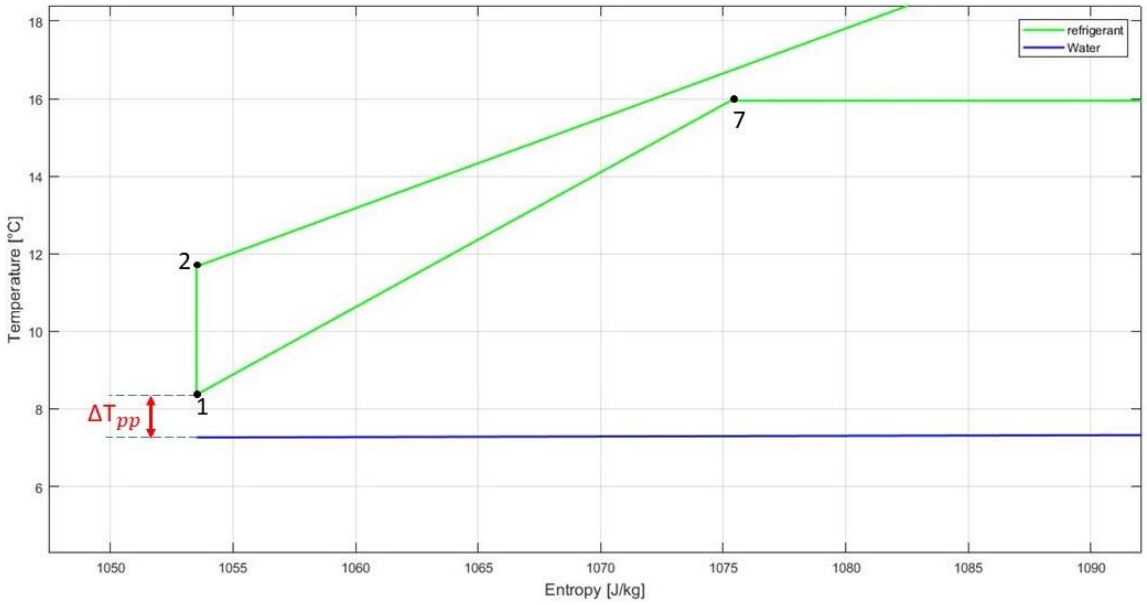

Figure 43. Detail on the pinch point.

The result can be explained by the fact that the tests carried out have never exceeded 12 kW of electrical power, while the condenser has been sized to work with a nominal power of 24 kW. It is, therefore, possible that increases in the value of the pinch point will occur when tests with higher powers will be performed.

Some final considerations can be made with reference to superheating. In the system examined in this study, the superheating phase is not present as the evaporator has been designed to return saturated steam. This sets a limit to the installation of a turbine with the purpose of producing electricity. Although it is an organic Rankine cycle, it is always recommended a certain superheat value when working with turbines as it allows to obtain a fluid at the end of the expansion further from the saturation conditions, avoiding the risk of droplets destructing the impeller blades. In order to work with turbines, therefore, it would be necessary to install a further section downstream of the evaporator capable of providing a certain level of superheat of the steam. The alternative to superheating consists in working with a volumetric expander since the latter components suffer less from corrosive phenomena.

3.8.4 Simulation

The analysis of the tests is concluded by simulating the presence of an expander machine with an isentropic efficiency of 75% (plausible value according to [23]), in order to obtain more tangible parameters, able to give us a clearer idea about the performances achieved by the system. In this way it is possible to calculate the theoretical power that would be generated and the efficiency of the system.

The cycle that would be obtained in a temperature-entropy diagram with the expansion of the fluid in the expander is as follows:

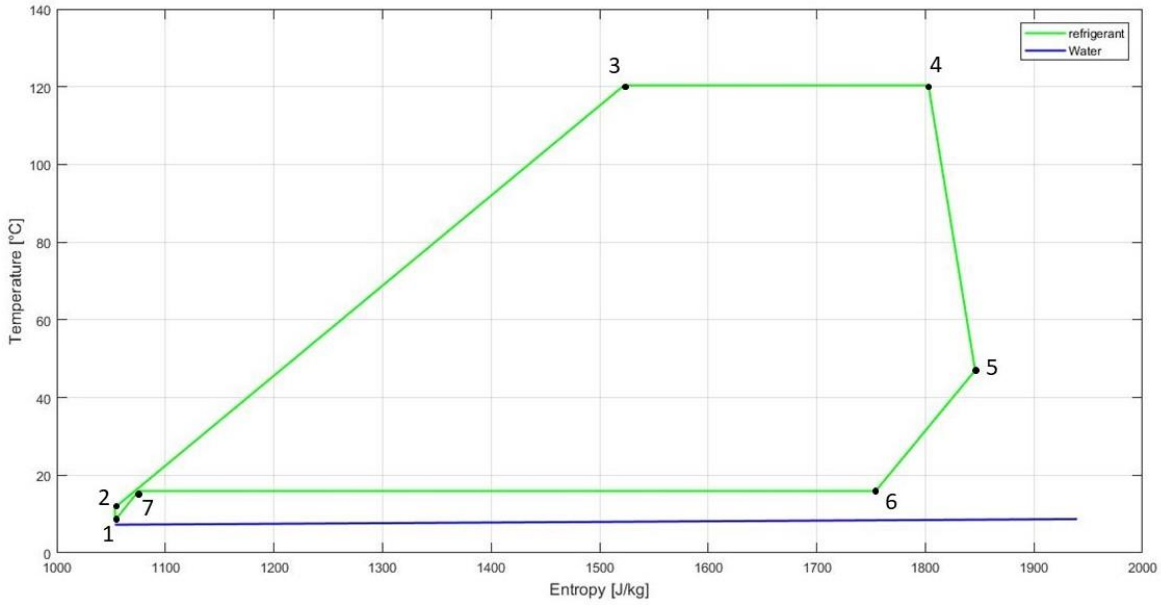

Figure 44. Simulated ORC on a temperature-entropy diagram

As already predicted when the performance of the organic Rankine cycle has been discussed (ORC performance, section 3.9.3), if we compare the two diagrams obtained without and with the expander (Figures 41 and fig 43) it is clear that in the second case the transformation 4-5 is much steeper and therefore the relative variation of entropy is smaller. Moreover, the temperature reached by point 5 is much lower than that reached in Figure (41), this is the consequence of the fact that in the expander the fluid undergoes an enthalpy decrease

between inlet and outlet. This variation of enthalpy corresponds precisely to the work for mass units, $\left[\frac{J}{kg}\right]$, that the expander is able to generate.

$$W_{exp} = \eta_{is} \cdot \left(h_{exp,su} - h_{exp,ex,is}\right) \quad (47)$$

Where

η_{is} is the isentropic efficiency of the expander, assumed equal to 0,75

$h_{exp,su}$ is the enthalpy of the fluid at the expander inlet, $\left[\frac{J}{kg}\right]$

$h_{exp,ex,is}$ is the enthalpy of the fluid at the expander outlet if the transformation were isentropic, $\left[\frac{J}{kg}\right]$

The theoretical power that would then be derived from the use of the expander is calculated as follows:

$$\dot{W}_{exp} = \dot{m} \cdot W_{exp} \quad (48)$$

The trend of the theoretical power generated as a function of the temperature at the evaporator outlet is shown in the figure:

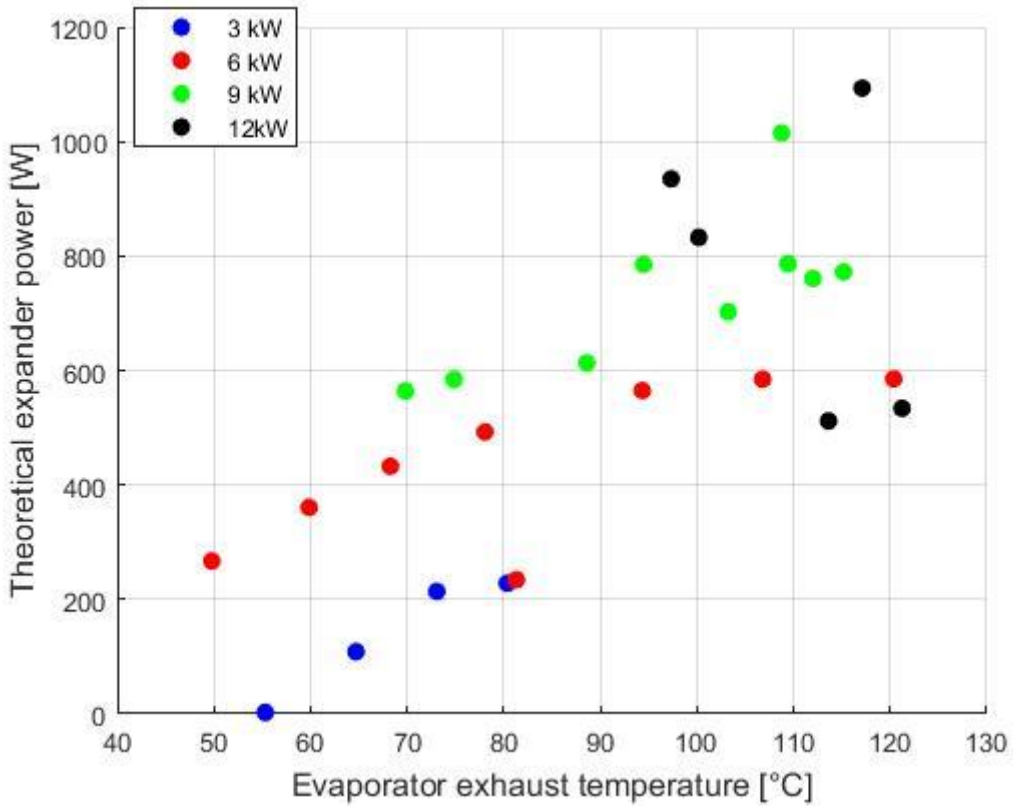

Figure 45. Theoretical expander power in function of the evaporator exhaust temperature.

The graph shows a clear positive trend of the power generated as the temperature increases in the evaporator. The same behaviour is also shown by the electric power used: the higher the electric power, the more theoretical power can be obtained from the expander. This is easily deducible also from the calculation of the theoretical power carried out with the equation (47). Generally, as the electrical power used increases, larger fluid flows can be developed, thus obtaining higher output power from the higher expander. It is interesting now to analyse the trend of the thermodynamic efficiency of the cycle as a function of the

temperature at the evaporator outlet and of the electric power used:

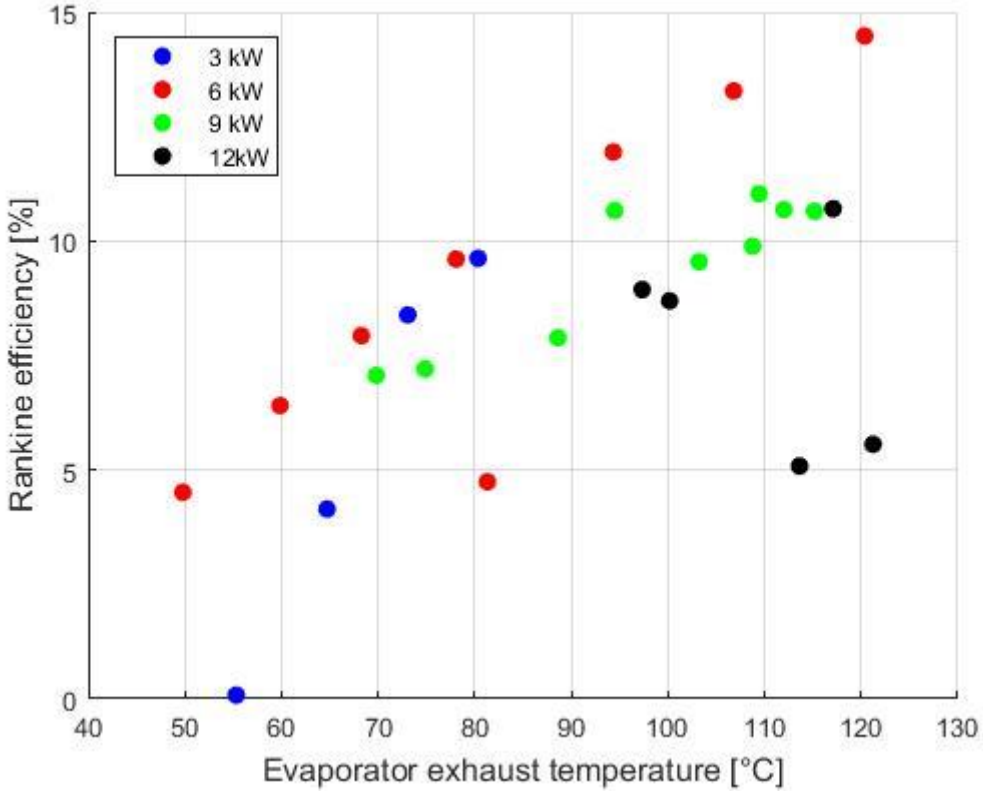

Figure 46. Thermodinamic efficiency of the Rankine cycle in function of the evaporator exhaust temperature.

The cycle efficiency has been calculated as follows:

$$\eta_{ORC} = \frac{\dot{W}_{exp} - \dot{W}_{pp}}{\dot{Q}_{el}} \tag{49}$$

The graph shows that good values of thermodynamic efficiency can be obtained (an efficiency of 14-15% is an excellent result for an ORC operating at such low temperatures) with the right combination of thermal power used and temperature at the evaporator outlet. To understand, however, why the maximum efficiencies have been obtained at an electrical

power of 6 kW and not at higher powers, it is necessary to examine the next graph:

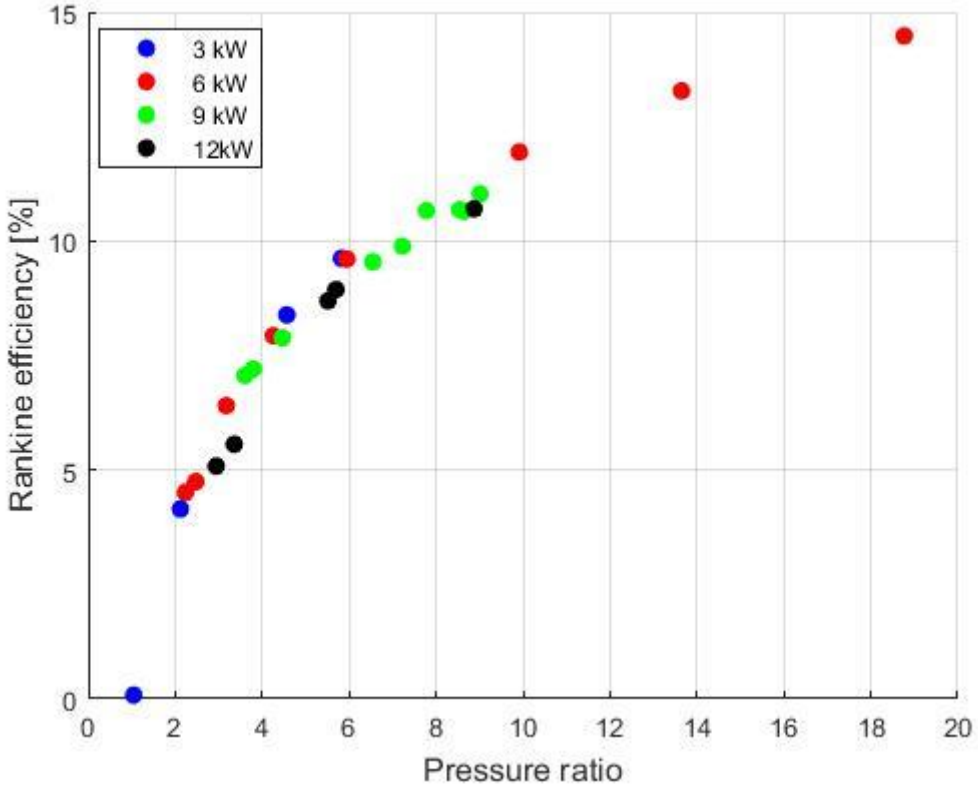

Figure 47. Rankine efficiency in function of the pressure ratio.

The graph expresses the efficiency of the cycle as a function of the pressure ratio (PR), defined as the ratio between the inlet and the outlet pressure of the expander:

$$PR = \frac{P_{exp,su}}{P_{exp,ex}} \tag{50}$$

As can be seen from the graph, there is a strong link between this parameter and efficiency since the PR is related to the enthalpy jump that can be processed by the expander. As already explained in section 3.9.2 and in particular in table 9, the operating limits set a maximum pressure in the order of 20 bar.

Therefore, two conclusions can be drawn:

- at the same pressure ratio, a better efficiency is obtained by using a lower electrical power

- in order to obtain higher efficiencies, it would be necessary to review the sizing of the most critical components in order to increase the pressure ratio that can be processed by the plant.

3.9 Conclusion and Perspectives

The experimental campaign conducted, has allowed obtaining useful data to characterize the behaviour of the system under different operating conditions and to identify the most critical parameters on which it is possible to intervene to achieve an improvement in performance. The evaporator, the component on which this analysis is based, has shown good performance especially in terms of pressure losses, which have been almost nil. The most critical aspect turned out to be thermal insulation since high heat loss values with the environment were recorded in all the tests performed. However, it is recalled that the experimental analysis has been largely limited by the anomaly related to the electrical resistances and that many aspects, therefore, need further investigations at higher powers. The level of liquid inside the evaporator, for example, has undergone great variations, approaching the maximum value on several occasions, especially for high flow and electrical power values used. The results showed that it is determined by a complex equilibrium dependent on several parameters and it was difficult to formulate a definitive conclusion. In the same way, when the presence of an expander was simulated, the best results in terms of efficiency were obtained at the intermediate power of 6 kW, while a gradual deterioration for higher powers was found. With regard to the overfilling of the evaporator, it has been deduced that it is difficult to make the system work under different power loads without a device such as a receiver, capable of storing part of the refrigerating fluid in circulation and thus avoiding imbalances in the load of the condenser and evaporator. The other solution hypothesized consists instead in reviewing the design of the evaporator by providing an enlargement of the tank placed in the upper part. Regarding the efficiency of the cycle, the factor that has most influenced the results has been the pressure ratio, as this determines the difference in enthalpy between the input and output of the expander. With increasing power, it has not been possible to increase the pressure at the evaporator outlet because of the limits imposed (above all on the temperature) nor it has always been possible to maintain the pressure at the input of the condenser at constant and low values. This led to a decrease in the pressure ratio and therefore in the thermodynamic efficiency of the cycle. In light of these considerations, it is clear that further tests at higher powers are necessary to confirm the hypotheses made and to gather a broader database of information. However, it is the author's opinion that some plant

limitations are already evident and that some interventions can be carried out before proceeding with a further experimental campaign, both to improve performance and to facilitate data acquisition. These improvements can be summarized as follows:

- Perform a correct heat insulation of the evaporator to reduce heat exchanges with the environment.
- Install a liquid receiver after the condenser to eliminate excessive liquid loads in the evaporator.
- To make automatic the acquisition of data related to refrigerant mass flow rate and liquid level inside the evaporator.
- Provide a control of the inverter in order to automatically regulate the rotational speed of the pump until the stabilization of the system is achieved.

One of the most interesting perspectives is to develop a model of the evaporator by adapting the thermosyphon model illustrated in chapter 2. This will allow simulations outside the operating conditions of the bench test, extrapolating results for higher powers and thus providing additional information on the feasibility of using this technology in industrial applications. It will also be possible to identify sources of losses more easily and to analyse in depth the operating limits linked to the two-phase closed thermosyphon technology (Dry-Out, boiling limits, sonic limits etc.).

In this dissertation, a first approach has been made to investigate the feasibility of using a thermosyphon heat exchanger for waste heat recovery. The simplified prototype that has been tested has shown promising results especially from the point of view of the critical aspects related to the particular geometry and the operating principle that exploits a fluid recirculation by means of gravity. After this analysis, it is clear that many aspects need further investigation, but the technology has proved promising for future developments in the field of industrial waste heat recovery using ORC systems.

Bibliography

[1] A. Barbotin, R. Cervi, O. Delabroy, G. Gouefelec and C. Lebrun, Performance enhancement of reheating furnaces using ocycombustion. AISE Annual Covention., Chicago, 2000.

[2] A. Foresti, D. Archetti and R. Vescovo, ORCs in steel and metal making industries: lesson from operating experience and next steps., Dusseldorf, Germany: METEC & ESTAD., 2015.

[3] Department G-RD, Energetic flowchart for cement, glass, steel industries and petrochemical sectors., 2015.

[4] G. Bonvicini, Heat recovery potentials in the most demanding processes., 2015.

[5] Turboden., Turboden Waste to Energy Solutions., 2016.

[6] C. Booth, L. Swanson and R. Taylor, Heat pipes for transferring heat to an organic rankine cycle evaporator, Google Patents, 2011.

[7] J. Gruss and P. Pardo, Systeme de récuperation de l'énergie de la chaleur de gaz chaud(s) et/ou fumée(s), application à la recuperation de l'énergie de fumées encrassantes, en particulier issues de moteurs thermiques, Google Patents, 2016.

[8] L. V. Long, S. Declaye, X. Dumas, L. Ferrand and V. Lemort, “Waste heat recovery by means of Organic Rankine Cycle (ORC) system coupled with two-phase closed thermosyphons,” *International Journal of Thermodynamics,* 2017.

[9] S. Quoilin, M. V. D. Broek, S. Declaye, P. Dewallef and V. Lemort, “Techno_economic survey of Organic Rankine Cycle (ORC) systes,” 2013.

[10] A. Amini, “"Heat pipe heat exchangers",” in *the 30th HEXAG Meeting*, Newcastle, UK, 2013.

[11] D. Reay, P. Kew and R. McGlen, Heat Pipes Theory, Design and Apllications, 2014.

[12] B. Marcia, Thermosyphon Technology for Industrial Applications. Heat Pipes and Solid Sorption Transformations: CRC Press, 2013.

[13] ESDU, Heat Pipes-Performance of two-phase Closed Thermosyphons, London, UK: Engineering Sciences, 1981.

[14] D. Isoppo, T. Borges and B. Marcia, "Development of a detailed thermal model for designing heat pipe heat exchangers.," in *22nd International Conference on Efficiency, Cost, Optimization, SImulation and Environmental Impact of Energy Systems.*, Foz do Iguacu, Parana, Brazil, 2009.

[15] D. Green and R. Perry, Perry's chemical engineer's handbook, McGraw-Hill, 2008.

[16] S. Klein, "EES: Engineering Equation Solver.," Academic P ed. Madison: F-Chart Software, 2013.

[17] A. Zukauskas, Heat Transfer from Tubes in Crossflow, Elsevier, 1972.

[18] M. Cooper, Saturation nucleate pool boiling - A simple correlation, Hewitt GF,Boland D, Bott TR, et al., editors, 1984.

[19] L. V. Long, X. Dumas, L. Ferrand and V. Lemort, "Modelisation d'un echangeur a thermosiphons pour la recuperation de chaleur," in *XIII Colloque Interuniversitaire Franco-Québécois sur la Thermique des Systèmes*, Saint-Lò, France, 2017.

[20] Tacmina, [Online]. Available: www.tacmina.com. [Accessed 20 February 2018].

[21] "Material Business Center," [Online]. Available: http://materialsbusinesscenter.se/open-innovation-portal/alfa-lava-antifouling/. [Accessed 20 February 2018].

[22] Meca-Fluid, "Brass Pressure Regulator up to 50 bar - R120 Datasheet," [Online].

[23] E. Macchi and M. Astolfi, Organic Rankine Cycle (ORC) Power Systems, Woodhead Publishing, 2017.

[24] Honeywell Refrigerants, "Honeywell-Genetron 245fa ORC systems brochure," [Online].

[25] KROHNE, “KROHNE Coriolis Mass Flowmeter OPTIMASS 6000-S15 Datasheet,” 2017. [Online].

[26] Bosch Rexroth, [Online]. Available: https://www.boschrexroth.com/en/xc/products/product-groups/assembly-technology/topics/aluminum-profiles-solutions-components/aluminum-profiles-products/index.